NATIONAL AND KAPODISTRIAN UNIVERSITY OF ATHENS
SCHOOL OF SCIENCE
FACULTY OF GEOLOGY & GEOENVIRONMENT

DEPARTMENT OF GEOPHYSICS & GEOTHERMICS

MINERALOGICAL AND GEOPHYSICAL INVESTIGATIONS ON THE TWIN-METEORITE IMPACT CRATERS IN THESSALY (CENTRAL GREECE)

Final Report

By

Lagios E., Dietrich V., Gartzos E., Sakkas V. & Reusser E.

Submitted to *John S. Latsis Benefit Foundation*

ATHENS
DECEMBER 2010

Mineralogical and Geophysical Investigations on the twin-meteorite impact craters in Thessaly (Central Greece)

By

Lagios Evangelos*, Dietrich Volker J.**, Gartzos Efthimios***, Sakkas Vassilios* & Reusser, Eric **

*Department of Geophysics & Geothermics, National Kapodistrian University of Athens, Panepistimiopolis Ilissia, Athens 157 84, Greece (lagios@geol.uoa.gr).

**Institute for Mineralogy and Petrography, Swiss Federal Institute of Technology, CH-8092 Zurich, Switzerland (volker.dietrich@erdw.ethz.ch).

***Laboratory of Mineralogy-Geology, Agricultural University of Athens, GR-118 55 Athens, Greece.

ΠΕΡΙΛΗΨΗ

Για πρώτη φορά παρουσιάζονται κρατήρες που έχουν αναγνωρισθεί στην Ελλάδα από πρόσπτωση μετεωρίτη. Δύο κυκλικές λίμνες διαμέτρου 150 και 250 μέτρων με αντίστοιχα βάθη 6 και 8 μέτρων και απόσταση περί τα 250 μέτρα μεταξύ των απαντώνται σε αγροτική περιοχή ΝΔ του Αλμυρού, στην Θεσσαλία. Η εν λόγω περιοχή είναι γνωστή και ως ο Προϊστορικός Μαγούλα-Ζερέλια Οικισμός, οποίος έχει κατοικηθεί από την Μέση Νεολιθική Περίοδο μέχρι την Εποχή του Χαλκού. Σύμφωνα με παλαιότερη αναφορά, "*Ο Ναός της Αθηνάς Ιτωνίδος ευρίσκεται σε μία από τις δύο λίμνες, ο οποίος έγινε αντιληπτός όταν η στάθμη της λίμνης έπεσε πολύ χαμηλά*", μετά από σεισμό το 1980.

Ο σχηματισμός των λιμνών με βάση τα πρόσφατα γεωμορφολογικά χαρακτηριστικά αποδίδεται στο Ολόκαινο και δύναται να περιορισθεί στο διάστημα πριν από 12500 έως 8000 έτη. Η θεώρηση ως προς την δημιουργία τους να οφείλεται ως το αποτέλεσμα πρόσκρουσης μετεωρίτη βασίζεται κυρίως στα σημαντικά και πολυπληθή ευρήματα από κροκάλες και λατύπες στο πηλώδες περιβάλλον των όχθεων των λιμνών αυτών. Οι εν λόγω σχηματισμοί ουδόλως έμοιαζαν με τους περιβάλλοντες σχηματισμούς ή έτερο άλλο ηφαιστειακό υλικό. Η πετρολογική, ορυκτολογική και γεωχημική μαρτυρία των συλλεχθέντων κροκάλων ως και των πολυγωνικών λατυπών οδήγησαν στην ερμηνεία του "ανθρακικού" υλικού το οποίο γενικώς ετήχθη και συνεπτύχθη λόγω υψηλότατης θερμοκρασίας από μεταμορφικό "σοκ" πρόσκρουσης μετεωρίτη. Από τις διαστάσεις των κρατήρων-λιμνών εκτιμάται ότι το μέγεθος των μετεωριτικών θραυσμάτων θα πρέπει να εκυμαίνετο μεταξύ 10-30 μέτρων πριν την πρόσκρουση αυτών στην επιφάνεια του εδάφους.

Λεπτομερειακές πετρολογικές και ορυκτολογικές εργαστηριακές έρευνες ικανού αριθμού δειγμάτων διαφορετικών διαστάσεων, σε συνδυασμό με την παρατηρούμενη εικόνα των αποτελεσμάτων από τις γεωφυσικές διασκοπήσεις, επιβεβαίωσαν την ως άνω θεώρηση περί πρόσκρουσης μετεωριτικών θραυσμάτων. Το πλέον πειστικό επιχείρημα στην προκειμένη περίπτωση συνίσταται στην εργαστηριακή μαρτυρία εύρεσης **μερικώς τετηγμένου ζιρκονίου** στα συλλεχθέντα πετρολογικά δείγματα, για την τήξη του οποίου απαιτούνται θερμοκρασίες μεγαλύτερες των 1400–1800 °C, οι οποίες όμως δεν απαντώνται σε διαδικασίες μαγματισμού και φαινόμενα μεταμόρφωσης στον Γήινο φλοιό και τον ανώτερο μανδύα.

SUMMARY

This is the first time that impact meteorite craters have been recognized in Greece. Two circular permanent lakes of 150 and 250 m in diameter and both 6 to 8 m depth, occur 250 m apart from each other in the agricultural fields SW of the town of Almyros (Thessaly). This picturesque site is known as the prehistoric Magoula Zerelia settlement, which was occupied from the Middle Neolithic period until Late Bronze Age. According to an older reference "the temple of *Athena Itonis* is situated in one of the two lakes and only visible when the lake falls dry" that only happened in 1980 after an earthquake. The formation of the lakes can be assumed on their fresh morphological character as Holocene age and may be bracketed between approximately 12 500 and 8000 years BP.

The working hypothesis of their origin due to meteorite impact was based on the finding a considerable amount of angular to rounded clasts and polygenic breccias in the sandy-silty clay of their shores as well as in their suspicious halos during reconnaissance investigations. All these rocks did not resemble either any of the surrounding rock formations or any volcanic material. The petrographic, mineralogical and chemical evidence of the collected clasts and polygenic breccias lead to the interpretation of the "carbonatitic" material as molten and quenched "impact fallback breccias and carbonatitic tectites" due high-temperature to shock-metamorphic meteoritic impact. According to the size of the crater lakes the dimensions of the meteorite, which might have split into two fragments, could have been about 10-30 m before reaching the surface.

Therefore, the major goal of the project was to find remnants of the meteorite, to investigate the underground structure of the lakes by geophysical methods in order to verify the hypothesis of their impact crater shapes and to find mineralogical evidence of high-temperature and high-pressures shock metamorphism.

Detailed petrographic and mineralogical studies (optical microscopy, scanning electron microscopy, Raman spectroscopy, X-ray diffraction) on a large number of samples from millimeter to decimeter rock size confirmed the previous results (spinifex carbonatites with feathery spinifex and spherulitic textures, glassy tektites, deformed and fragmented quartz crystals) and thus evidence for shock-metamorphism and melting. The most convincing evidence is the finding of partial melted zircon, for which temperatures greater than 1400°–1800°C are required, which do not occur in metamorphic and magmatic process in the Earth's crust and uppermost mantle.

CONTENTS

INTRODUCTION

Since the 1960s, geologists started to realize the geological importance of meteorite impact events, especially the rare catastrophic collisions of kilometer-sized asteroids and comets, which have significantly shaped the Earth's surface (Shoemaker 1961; von Engelhardt & Stöffler 1965, 1968; Alvarez et al. 1980 , 1995; Alvarez 1997; French 1998), changed the atmosphere and climate for a long time, and disturbed to a large extend the entire biological cycle and evolution. The record of impacts on Earth is still being deciphered. Up to now, 178 individual geological structures have been identified as the preserved results of impact events worldwide (compilation in Osinski et al., 2008; French, 1998 and in the "Earth Impact Database"); only 37 craters in Europe, mainly in geological old crystalline basement in Sweden and Finland, only 2 in southern Germany and 1 in France, none in the entire Mediterranean. The known impact craters range from small circular bowls (partially as lakes) only a few kilometers or less in diameter to large complex structures more than 200 km in diameter and as old as 1 Billion years.

This is the first time that impact meteorite craters have been recognized in Greece. Two circular permanent lakes of 150 and 250 m in diameter and both 6 to 8 m depth, occur 250 m apart from each other in the agricultural fields SW of the town of Almyros (Thessaly). This picturesque site is known as the prehistoric Magoula Zerelia settlement, which was occupied from the Middle Neolithic period until Late Bronze Age. According to an old story by Theocharis "the temple of Athena Itona is situated in one of the two lakes and only visible when the lake falls dry", which only happened in 1980 after an earthquake (Reinders et al., 2004).

The working hypothesis of their origin due to meteorite impact was based on the finding a considerable amount of angular to rounded clasts and polygenic breccias in the sandy-silty clay of their shores as well as in their suspicious halos during reconnaissance investigations. All these rocks did not resemble either any of the surrounding rock formations or any volcanic material. The petrographic, mineralogic and chemical evidence of the collected clasts and polygenic breccias lead to the interpretation of the "carbonatitic" material as molten and quenched "impact fallback breccias and carbonatitic tectites" due high-temperature to shock-metamorphic meteoritic impact. According to the size of the crater lakes the dimensions of the

meteorite, which might have split into two fragments, could have been about 10-30 m before reaching the surface.

Therefore, the major goal of the project was to find remnants of the meteorite, to investigate the underground structure of the lakes by geophysical methods in order to verify the hypothesis of their impact crater shapes and to find mineralogical evidence of high-temperature and high-pressures shock metamorphism.

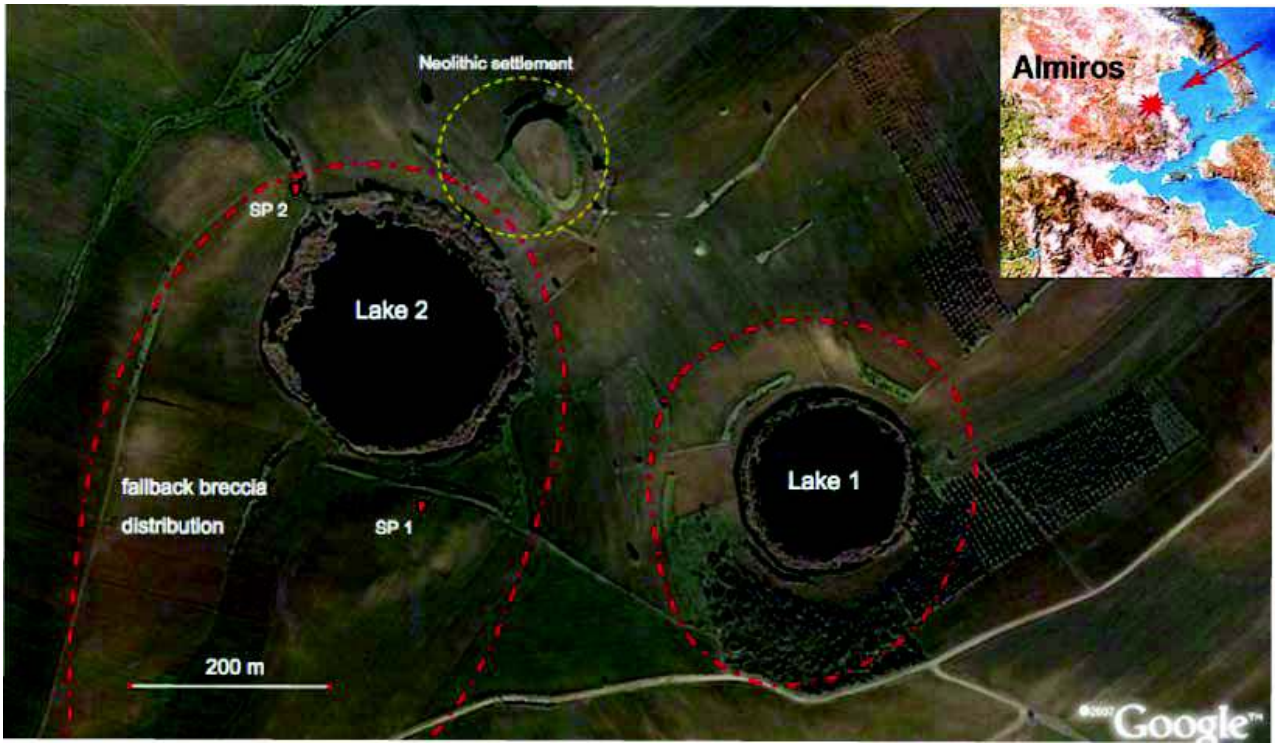

Figure 1 The Magoula Zerelia twin-lakes in the agricultural fields SW of the town of Almyros (Thessaly) with the hillsite of the prehistoric Magoula Zerelia settlement, which was occupied from the Middle Neolithic period until Late Bronze Age. Red stippled line mark the distribution of the "fallback breccia" as deposits due to the impact of the projects. SP 1 and 2 mark sampling points at small trenches within the walls of the fallback breccias.

Proposed work:

- Dredging and piston core sampling of lake bottom sediments
- Sedimentary research in nearby river and creeks for deposition of impact back fall spherules and tectites
- Mineralogical investigations: determination of crystallographic, chemical composition of new-formed minerals during within the ejecta with XRD, electron microprobe and Raman spectra methodologies.
- Magnetic and gravity investigation of the deeper structure of the crater lakes
- Possible recognition of remnant meteorite fragments at depth
- Search for fragmental meteoritic shards in the surrounding walls and fields

CHAPTER 1

ENVIRONMENTAL AND GEOLOGICAL SETTING

1.1. ENVIRONMENTAL AND GEOLOGICAL SETTING

The Magoula Zerelia twin-lakes in the agricultural fields SW of the town of Almyros. The basement beneath the alluvial cover consists of Cretaceous marly limestones, schists, phyllites, cherts, as well as of slices of radiolarites, serpentinites and meta-basalts (Geological maps of Greece, 1 : 50 000, sheet Anavra, Marinos et al. 1957 and sheet Almiros, Marinos et al. 1962). The lakes were regarded as dolines due to the occurrence of karst phenomena in equivalent rock formations in the surrounding Othris mountains. Another hypothesis as volcanic “maar-type diatremes” has been suggested on the basis of the existence of small Cenozoic volcanic centers in the wider area between Volos and Lamia (Marinou, 1962), however without any evidence for ejected volcanic material.

The ages of the lakes can be assumed on their uneroded morphological character as Holocene and may be bracketed between approximately 12 500 and 9000 years BP; the latter age according to the Middle Neolithic settlement on the hill between the two lakes (Fig. 1 and 2).

The two lakes represent a remarkable phenomena, with the exeption of two small springs (Kefalosis near “tsifliki Dhoukas” and near the Mavrolofos bridge) no natural water sources are available in the southern part of the Almiros plain. The lake never fall dry since many generations according to oral information of the farmers; with one exception after an earthquake in 1980.

The only explanation is, that their underground consist of clays and marls within a bowl shape structure, which prevents drainage of water. Lake 2 shows only a small stream at the southern rim (Fig. 3) and a small spill and creek at the northeastern rim, controlling an overflow during seasonal flooding due to thunderstorms. A sedimentological study on mud piston cores from the ground of the lakes yielded sedimentation rates of unconsolidated sediments range in the order of 0.4-0.5 cm/year according to isotopic Cs and Pb dating (Keller, 2010).

Such a situation excludes practically the interpretation of an origin of the lakes as karst dolines.

Figure 2. Magoula Zerelia lake 1

Figure 3 Magoula Zerelia lake 2. In the background Orthris mountains.

1.2. FIELD-WORK CAMPAIGNS

1.2.1 November 14 and 15 2009: Piston core sampling of lake bottom sediments.

Figure 4. Piston-Core sampling locations

Figure 5. Lake 2 with Piston-Core sample. Depth of Lake 2 ca. 6-7 m. Unoxic conditions. (Efthimios Gartzos, AUA)

Figure 6. East Lake 1 with Piston- Core sample. Depth of Lake 1 ca. 7 m. Description of Piston- Cores performed within a student-work by Mr. Mirco Keller (Environmental Sciences, Swiss Federal Institute of Technology Zurich, May 2010).

1.2.2. March 1/2, and April 25/26 2010: Sampling of impact back-fall breccia Lake 2 for petrographic and mineralogical studies and for optically stimulated luminescence (OSL) age determination (Duller, 2004) of the impact.

Figure 7. Conventional sampling method of a large soil sample from the South wall Lake 2 (SP 1, Fig. 1) in order to avoid sunlight penetration. Only the center of the sample ill be processed for OSL age determination (Konstantionos Kyriakopoulos, NKUA).

Figure 8. New sampling method of Drill core soil sample from the North wall Lake 2 (SP 2, Fig. 1) in order to avoid sunlight penetration. Only 10 cm of the center of the core will be processed for OSL age determination.

1.2.3. April 25/26, 2010: Magnetic investigation of the deeper structure of the crater lakes in order to detect possible meteorite fragments at depth.

Figure 9. Magnetic survey around Lake 1 with portable magnetometer and GPS positioning (Vangelis Lagios, left and Vassilis Sakkas, right, NKUA)

CHAPTER 2

PETROGRAPHY AND MINERALOGY

Although both lakes show very similar morphological and structural characteristics the material comprising their walls differ significantly.

2.1. ROCK MATERIAL AROUND LAKE 1

The soil as well as the walls of the smaller lake 1 (area outlined in Fig.1) are composed of white to yellowish carbonates with grainsizes from sand to clasts of several centimeters in diameter. All rock pieces exhibit irregular angular to subrounded shapes, full of cavities and contain few but distinct fragments of reddish radiolarian cherts (Plate I). Fragments of limestones, cherts, shales and shists, similar to those of the Cretaceous country rocks, are rare.

Figure 10. Zerelia lake 1 with the view towards NE into the plain of Almiros and Pagasitigos. No outcrops are exposed within the smooth walls (halo) around the lake.

The textures and mineralogy of the rock material will be described in section 2.3.

Plate I Fallback impact breccia Zerelia lake1

A Casts of fossiliferous limestone (FL), carbonate veins

B Clasts of fossiliferous limestone (FL) in reddish carbonate matrix

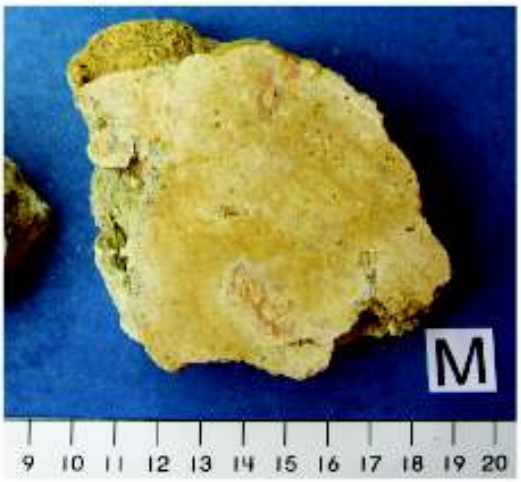

C

„Cauliflower clast"
Recristallized fossiliferous limestone with infiltration of iron-rich carbonate matrix

D Breccia clasts of porous carbonatitic carbonates and euhydral calcite crystals in veins

E Breccia clsts with reddish carbonatitic spinifex textures and euhydral calcite crystals in veins

2.2. ROCK MATERIAL AROUND LAKE 2

The area outlined in Fig. 1 around the two lakes are covered with irregular, angular to sub-rounded rock pieces, which vary in size from micron through millimetre and centimetre up to block sizes of approximately 10-20 cm (Fig. 11 and 12). Their colours vary from light yellow to dark yellow, orange and yellow-brownish. However, their yellowish to reddish fine-grained marly sandy matrix (<0.2 to 2mm grain size) seems to be in general similar and consistent in composition. This material builds up flat walls as halos around the lakes (Fig. 1, 7, 8, 11 to 15; Plates I-XI). Two localities, north and south of lake 2 (sampling localities SP1 and SP2, Fig. 1, 8 and 13) permit an inside of the walls of approximately up two meters depth. These sections exhibit the same chaotic appearance of rock detritus as the surface and do not show any effects of sedimentary structures, such as sorting or layering.

The larger brecciated clasts differ highly from one to each other concerning their internal fragmented polygenetic rock material. The textures and mineralogy of the rock material will be described in section 2.3. SHOCK-METAMORPHIC EFFECTS IN ROCKS AND MINERALS.

Apparent is, that practically NO limestones, which build up in general the underground of the vicinity, neither are found inside the “fallback distribution area” (Fig. 1) nor as components inside the consolidated brecciated rock pieces.

Figure 11 Southwest wall Lake 2 covered by back-fall impact breccia and sand of grain sizes from micron to blocs of several decimeters.

Figure 12. Surface of Lake 2 wall with fallback impact breccia breccia with abundant quartz and chert fragments embedded in a carbonatitic, marly soil.

Figure 13. Small crosssection in the southwall of lake 2 (sampling point SP1 in Fig. 1). Chaotic distribution of rock detritus without significant sedimentary structures, such as sorting or layering.

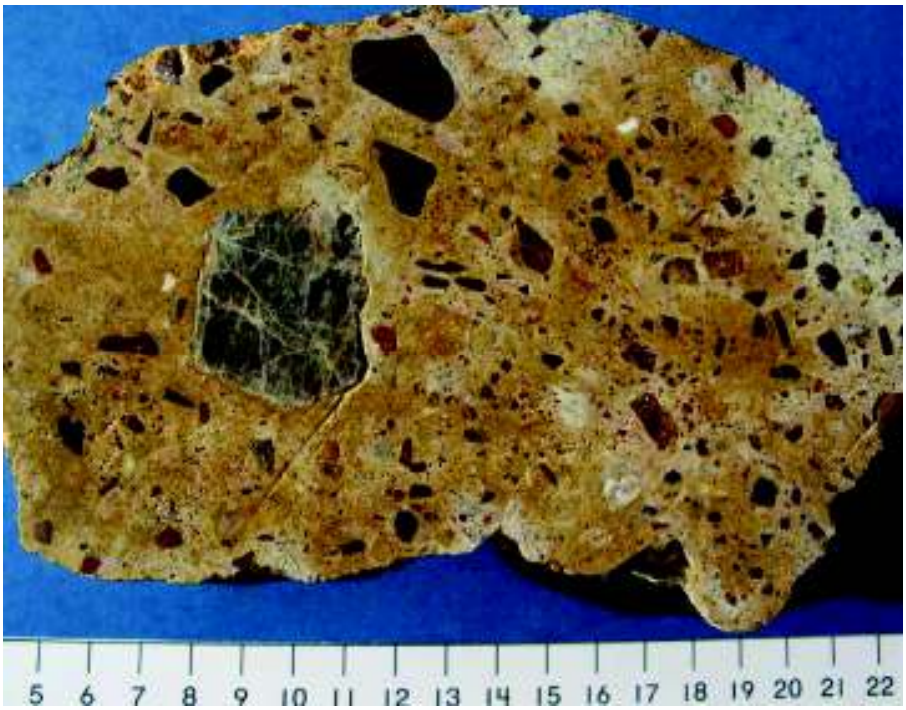

Figure 14 Polygenic impact breccia type A, lake 2. Broken fragments of quartz and reddish to brownish radiolarian cherts (SiO_2) are distributed chaoticly in a fine-grained calcite matrix with aboundant feathery spinifex textures (Plate IVb).

Fig. 15 Polygenic impact breccia type B, lake 2. Broken fragments of quartz and reddish to brownish radiolarian cherts (SiO_2) yellowish carbonatitic components (matrix of breccia type A) distributed chaoticly in a fine-grained spherulitc calcite matrix (Plate V).

Plate II Fallback impact breccias of Zerelia lake 2

A Carbonatitic clast with radiolarian cherts in patchy spinifex calcite matrix

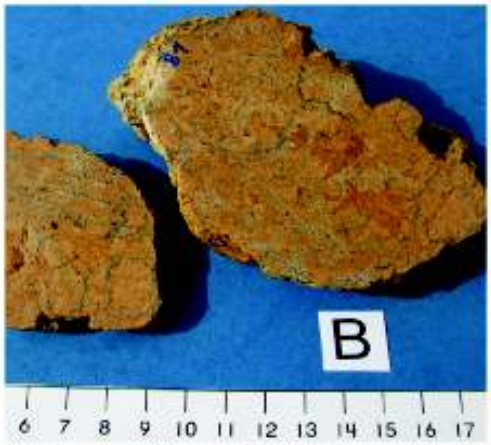

B Carbonatitic clast with dissiminated veins in patchy spinifex calcite matrix

C Carbonatitic clast with calcite veins and glass shards in spinifex calcite matrix

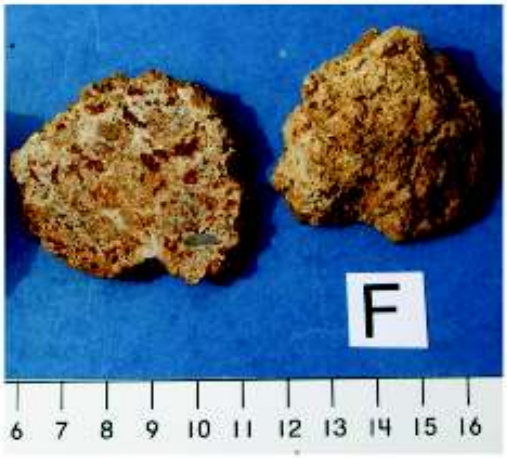

D Carbonatitic clast with dissiminated calcite veins in microcrystalline matrix

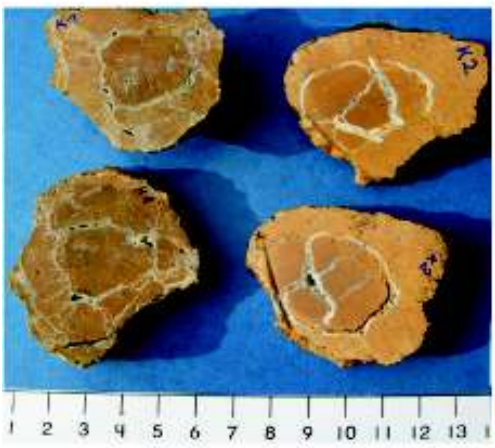

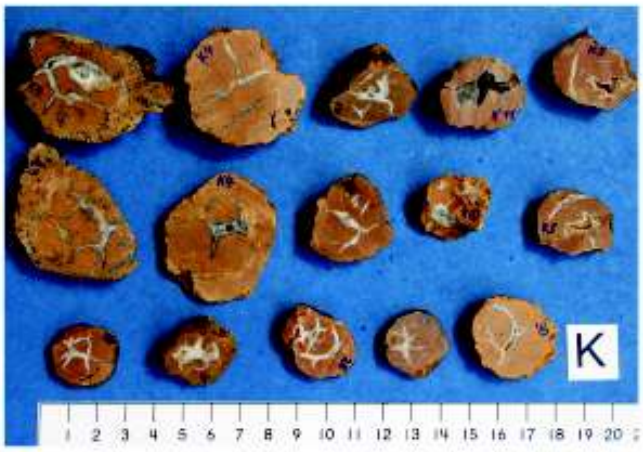

E & F Carbonatitic clasts ("impact backfall lapilli") with euhedral concentric and radial calcite fillings in microbrecciated, microcrystalline, patchy and coarse spinifex matrix

2.3. SHOCK-METAMORPHIC EFFECTS IN ROCKS AND MINERALS

The recognition since the 1960s of meteorite impact events (von Engelhardt & Stöffler 1968), and the increasing number of impact structures still preserved on Earth, is the result of two related physical processes: (1) The extreme physical conditions that affect the Earth crust by strong shock waves during impact and which can be recognized as durable **shock-metamorphic effects**; (2) such strong shock waves are produced only by hypervelocity impacts of extraterrestrial meteorites. Shock-metamorphic effects in rocks and minerals are critical to the identification impact structures, their size and physical conditions of the impact. The kind of shock-metamorphic effects (deformation, melting and recrystallization) depends highly on the physical conditions, pressure and temperature generated during the impact, which are related to the size and kind of the meteorite and its velocity.

Several characteristic shock-metamorphic effects can be distinguished in the rock material around the Zerelia lakes. Evidence for impact melting of carbonates, shales, shists and cherts of the surrounding country rocks is based on: (1) groundmass-forming calcite within fallback impact breccias exhibiting quenched feathery spinifex textures, (2) irregular shaped clasts and globules ("impact lapilli") and (3) individual small broken subrounded to angular particles and spherules of quartz and cherts. One of the most convincing evidence for identification of impact craters are relicts of impact melts: discrete, small (millimeter- to centimeter-sized), irregular, generally glassy objects in the fallback deposits around the craters (Langenhorst et al. 2000; Osinski et al. 2005 & 2008).

2.3.1 Quenched feathery spinifex textures (Plates III a and b, V)

The homogeneous carbonatitic grains (globules ans spherules) and clasts display distinctive feathery to coarse spinifex textures of calcite. These crystal aggregates are coarser towards the inner parts and progressively finer towards the rims. In addition, fine spinifex crystals cover the matrix and outer rims of "impact fallback lapilli" radial and concentric cracks, which originate from the inner parts of the lapilli and are filled with euhedral calcite (Plate II E & F, Plate IV F). Many fine spherules (< 100 mm to a few mm) are entirely filled with patchy feathery calcite (Plate III B & PlateV

F).

Plate IIIa contains thinsection microscopic images of spinifex textures of carbonatites from Zerelia lake 1, which show spinifex crystalgrowth of calcite from a microcrystalline “fluidal” and network state to fine spinifex aggregates.Plate IIIb Spinifex shows textures of carbonatites from Zerelia lake 2.

Plate IIIa Spinifex textures of carbonatites from Zerelia lake 1

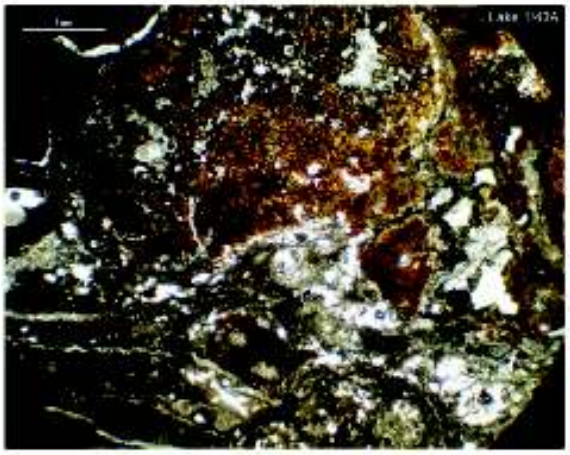

A Porous carbonatitic clast; microcrystalline fluidal calcite spinifex matrix

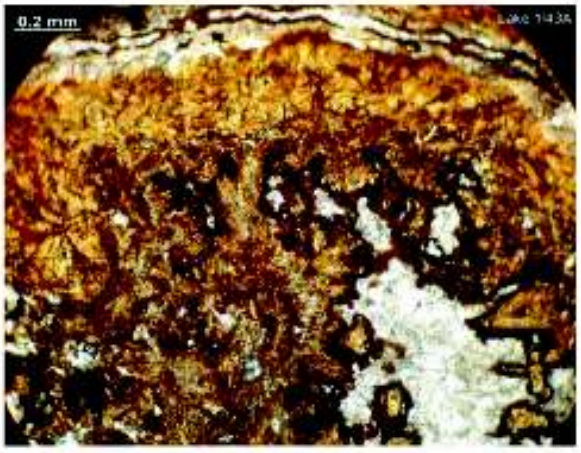

B Detail from A; microcrystalline fluidal calcite spinifex matrix; euhydral calcite fillings and fine reaction rims

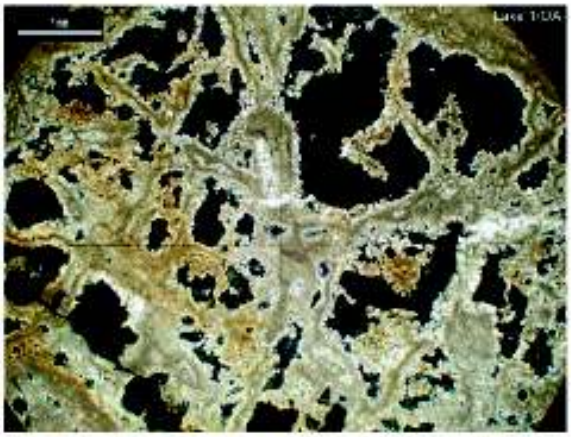

C Spinifex crystalgrowth from a network of microcrystalline calcite veins

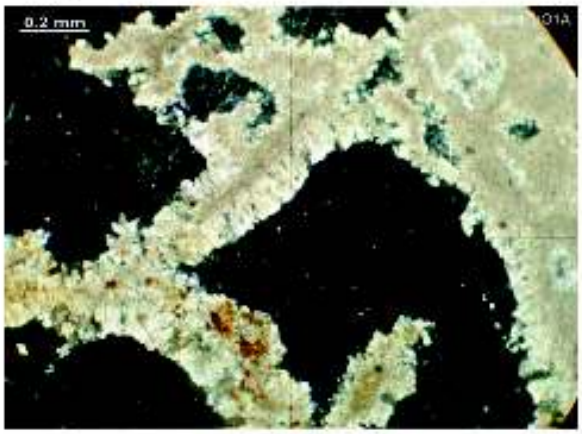

D Detail from A, spinifex crystalgrowth

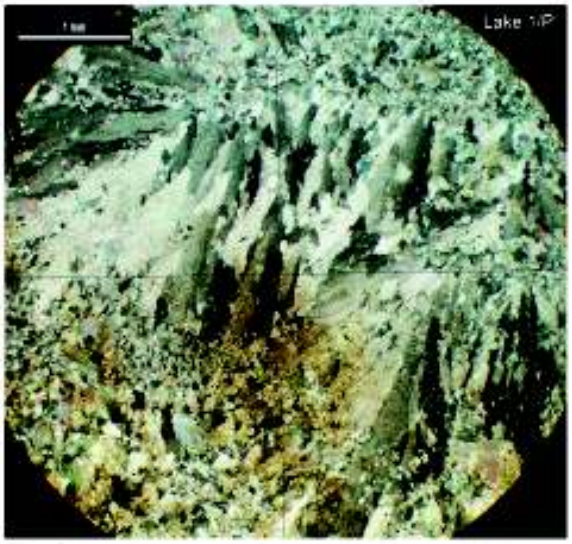

E Crystallgrowth of spinifex calcite including small quartz clasts

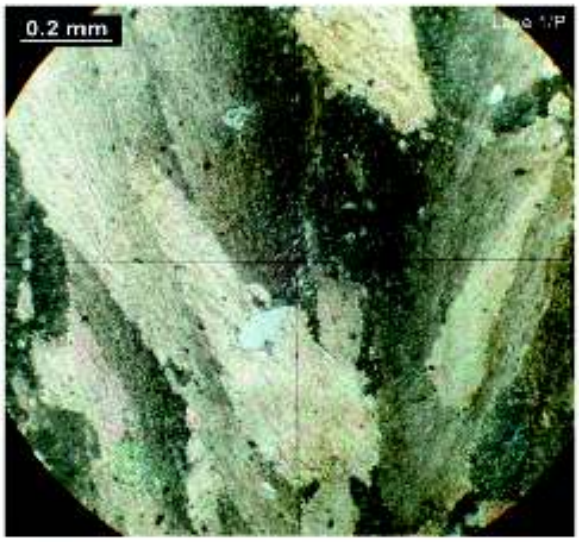

F Detail of crystallgrowth of spinifex calcite including small quartz clasts

Plate IIIb Spinifex textures of carbonatites from Zerelia lake 2

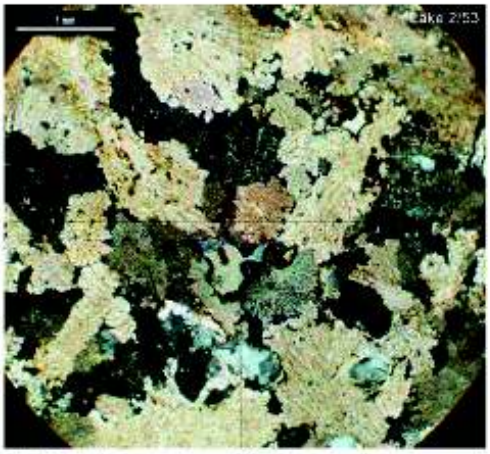

A Patchy carbonatitic groundmass spinifex calcite and small quartz clasts

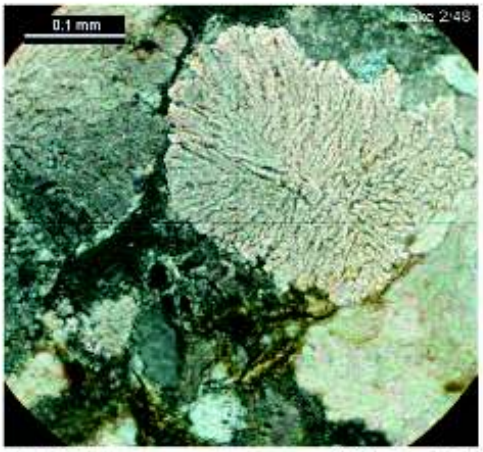

B Patchy groundmass spinifex calcite with radial crystallization

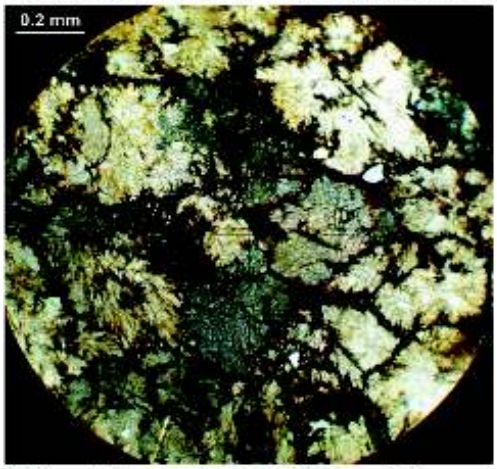

C Crystallgrowth of spinifex calcite with opake interstitial filling

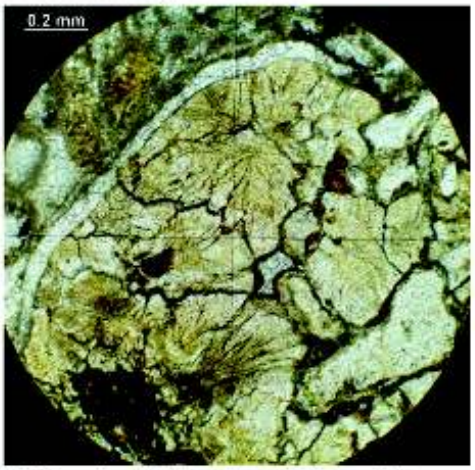

D Small spinifex clast with calcite reaction rim in spherulitic breccia

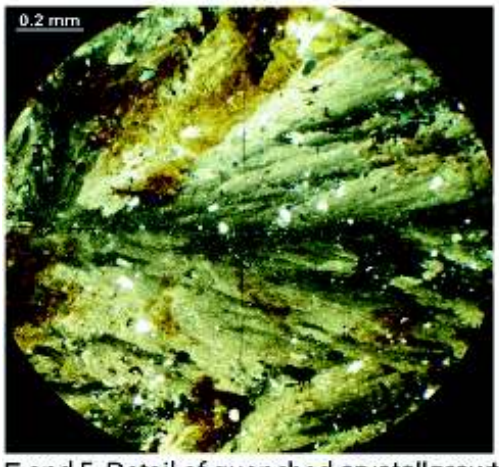

E and F Detail of quenched crystallgrowth of spinifex feathery calcite with undulate extinction including small quartz clasts (under crossed polarized light)

2.3.2. Globule clasts ("backfall impact lapilli"), Plate IV

Globule clasts ("backfall impact lapilli") were found after washing large samples of unconsolidated clastic fallback material in the sampling locality SP1 in the south wall of lake 2. Their grain size comprizes a few millimeter. Six typical selected varieties are shown in Plate IV: (A) concentric micobreccia globule with decomposed "glassy" silicate/carbonate groundmass, (B) opake micocrystalline, micobreccia globule, and four (C – F) different microbreccia, microcrystalline to micro-spinifex globules.

2.3.3. Spherules in fallback impact breccias of Zerelia lake 2, Plate V

Many fine-breccias contain numerous carbonate spherules, which occur as individual spherules and show in several cases coalescent bounding. Some of the spherules contain cores of quartz, chert and spinifex carbonate fragments. In most cases the spherules display reaction rims and coronas of submicroscopic fine carbonatic mineral assemblages. These spherules are not "secondary vesicle fillings", since they are made up of cryptocrystalline to microcrystalline and fine-grained euhedral carbonates with "schlieren" and spinifex textures.
The interstitial matrix consists of fine- to coarse grained euhedral calcite crystals.

2.3.4. Melted zircon in tectites from Zerelia lake 2, Plate VI

A few several millimeter size globules are made up of dense submicroscopic, kryptocrystalline "porcellan-like" hard matrix. We interpret these globules as carbonatitic tectites. Small irregular shaped zircon grains with bulged rims, incorporated into "altered" impactmelt glass from preimpact target rocks, are seen as partial melted crystals. According to SEM/EDAX analyses the grains contain irregular disributed areas of partial decomposition of the zircon ($ZrSiO_4$) to baddeleyite (ZrO_2) while the core of the grain consists of unaltered zircon (gray).

2.3.5. Mineral and fluid inclusions in quartz from impact breccias, Plate VII and VII

Small mineral and fluid inclusions occur often in quartz crystals. Predominatly, inclusions are abundant in idiomorphic quartz from spherulitic impact breccias. Calcite is the most common phase, followed by apatite, rutile, ilmenite, alkalifeldspar, muscovite and phlogopite.

Plate IV Globule clasts ("backfall impact lapilli") Zerelia lake 2

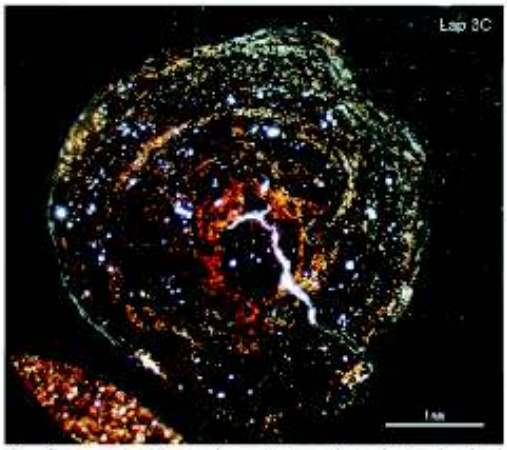

A Concentric microbreccia globule in „decomposed glassy" matrix

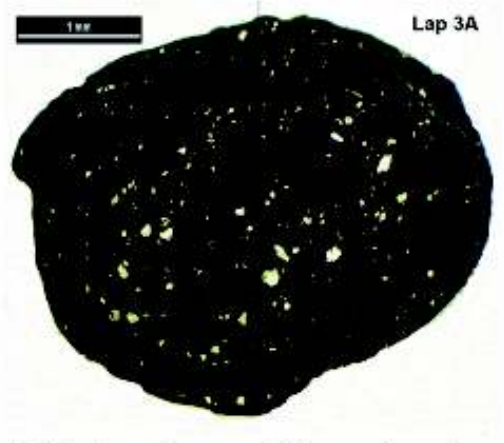

B Opake micocrystalline and partly glassy microbreccia globule

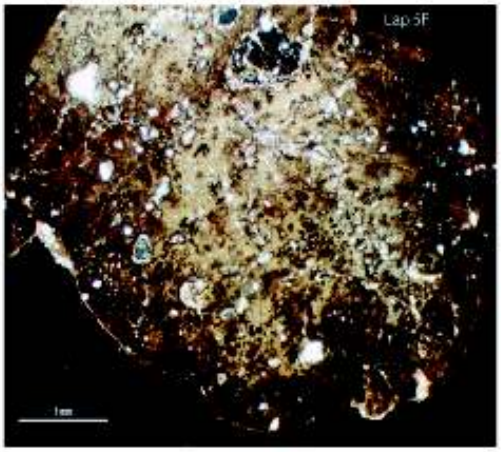

C Carbonatitic microbreccia globule in microcrystalline calcite matrix

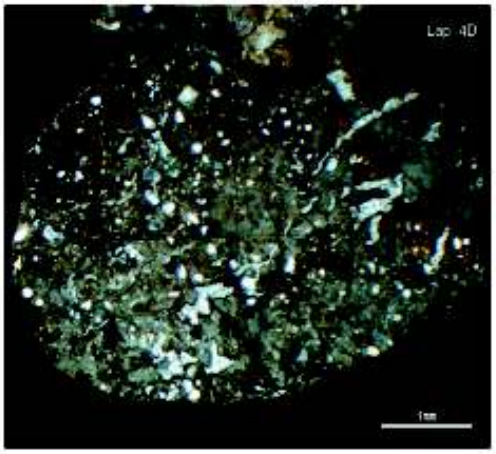

D Microbreccia globule with calcite veins in porcellane matrix

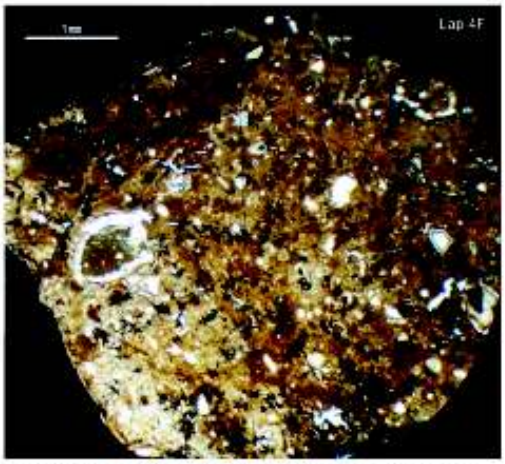

E Carbonatitic microbreccia globule in microcrystalline Fe-rich calcite matrix

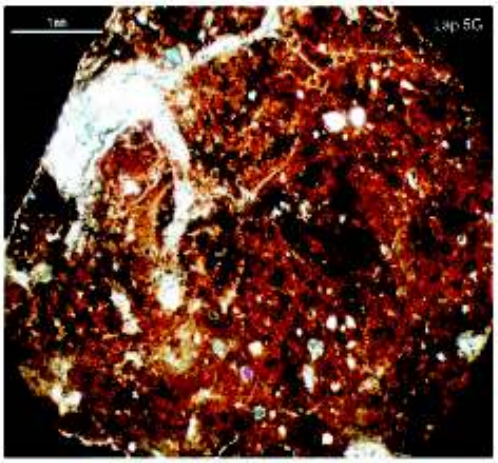

F Carbonatitic microbreccia globule in microcrystalline Fe-rich calcite matrix

Plate V Spherules in fallback impact breccias of Zerelia lake 2

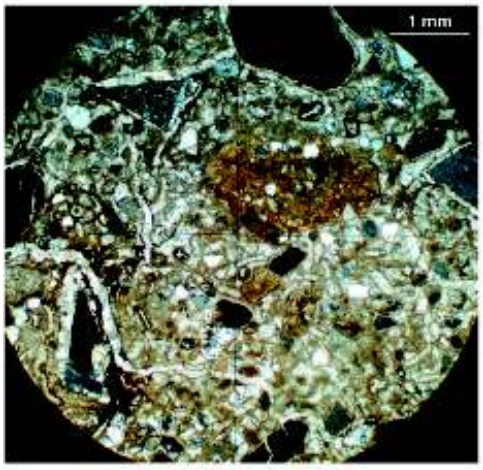

A Spherulitic clast with microclasts of quartz, cherts, calcite spinifex clasts

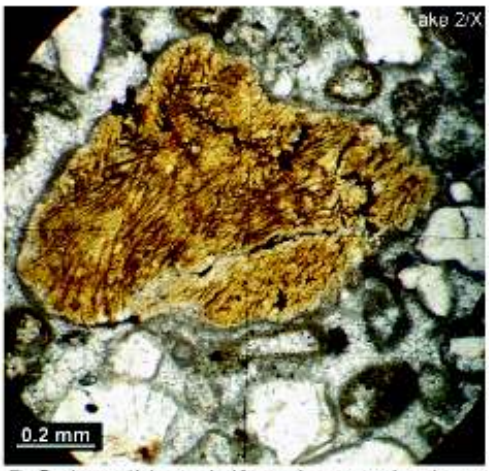

B Spherulitic spinifex clast and micro-cristalline calcite spherules

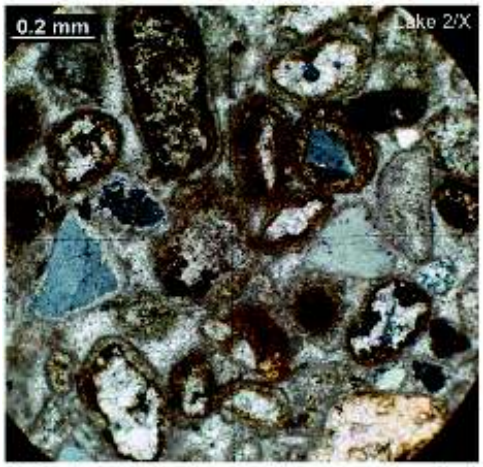

C Spherulitic clast with microclasts of quartz (grey), calcite spherules

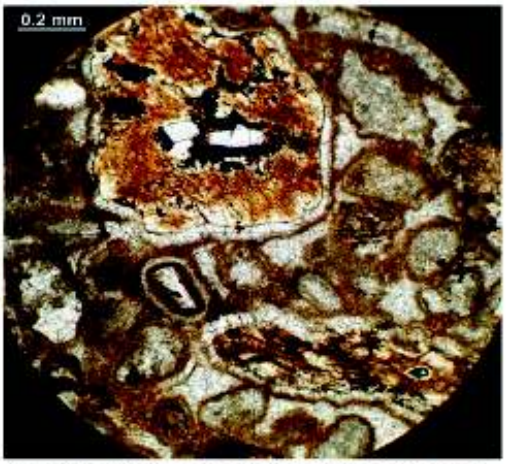

D Spherulitic spinifex clast and micro-cristalline calcite spherules

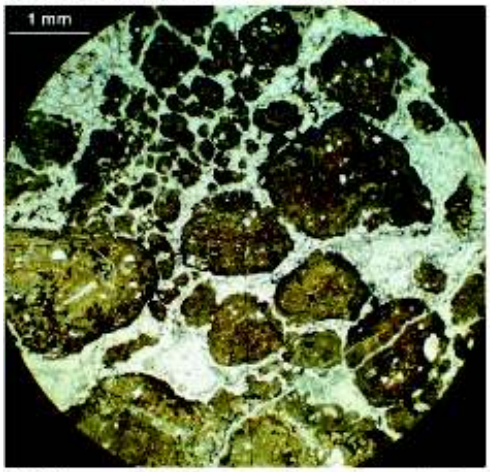

E Microcristalline calcite spherules in euhedral calcite matrix

F Coagulating microcristalline calcite spherules in euhedral calcite matrix

Plate VI Melted zircon in tectites from Zerelia lake 2

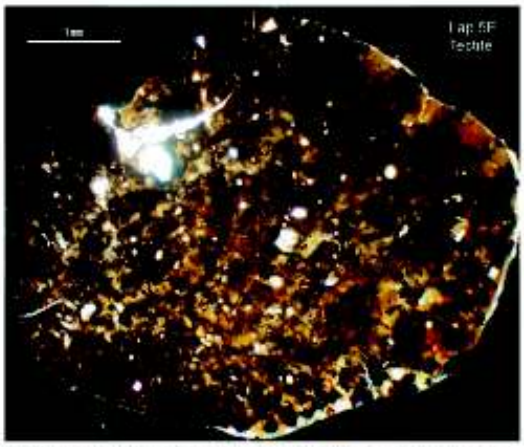

A Impact tectite with „porcellane" micro-breccia matrix icluding micro quartz clasts

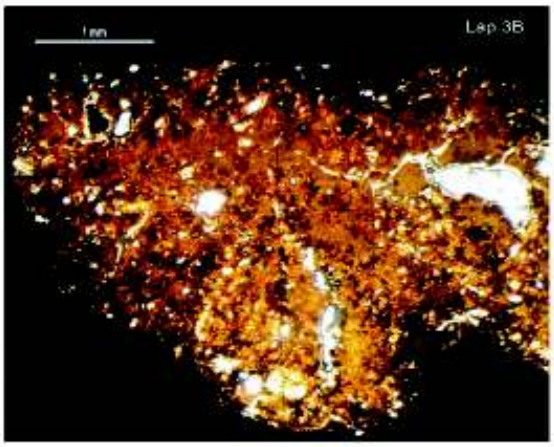

B Impact tectite with „porcellane" micro-breccia matrix and euhedral calcite veins

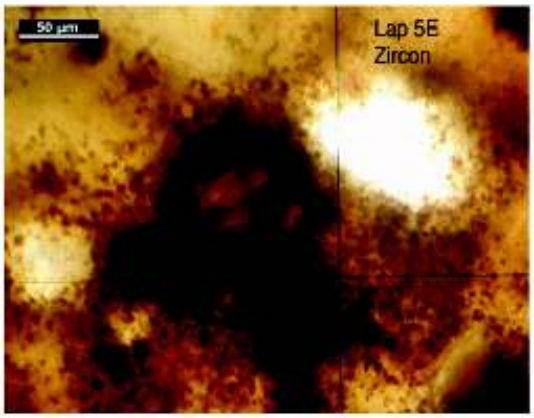

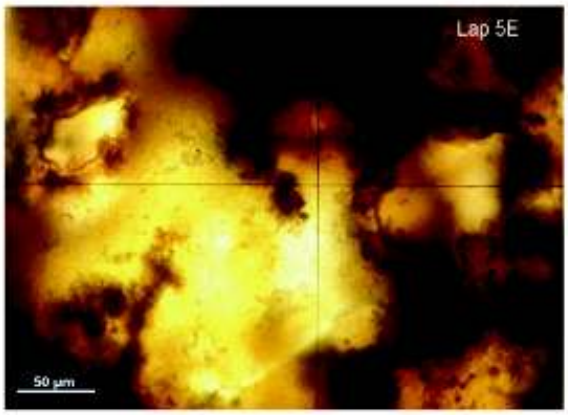

Remnants of melted zircon with reation rims in impact tectites (pictures A and B respectively)

Melted zircon in tectites and impact brecciain impact craters

High-temperature effects; melted (decomposed) zircon into a granular aggregate of the mineral baddeleyite (ZrO_2) (small bright dots) and silica glass (grey); Aouell-oul Crater (Mauritania). Decomposition at experimental temperatures of 1750°C.

Zircon Grain from Lunar Breccia 72215

(Photomicrograph courtesy of Alex Nemchin, Curtin University of Technology, Australia.)

Partial melted zircon from lunar impact breccia. Taylor (2009)

Plate VII Mineral and fluid inclusions in quartz from impact breccia

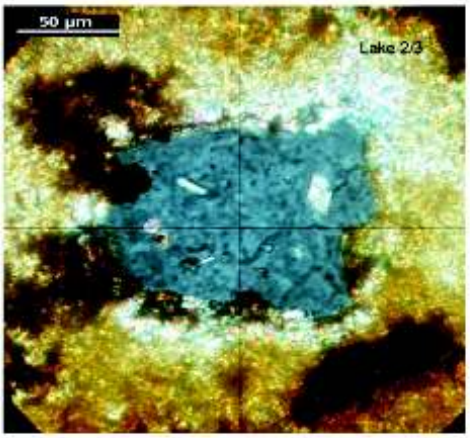

A Quartz fragment with calcite, apatite, feldspar and fluid inclusions

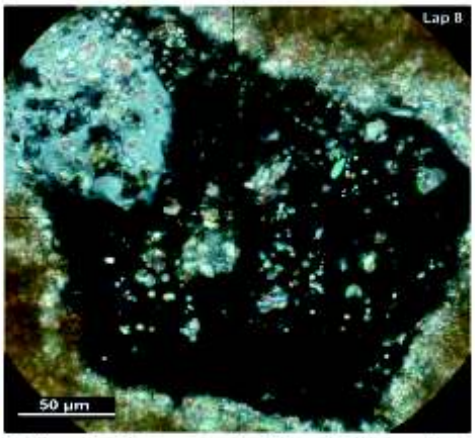

B Quartz fragment with calcite and fluid (CO_2 etc.) inclusions

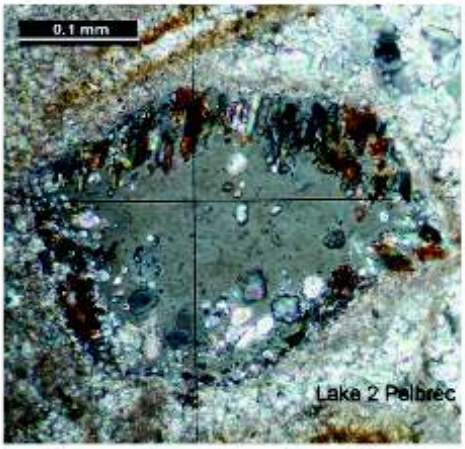

C Idiomorph quartz with calcite, apatite, ilmenite, rutile and fluid inclusions

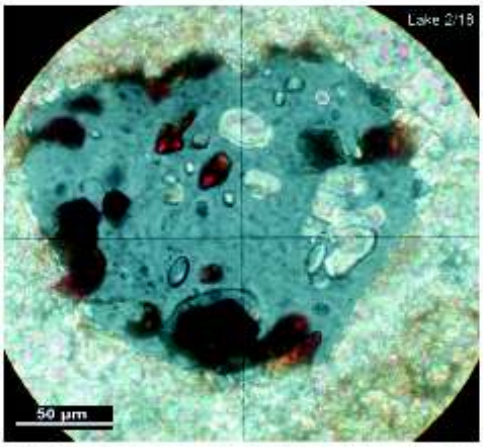

D Quartz fragment with calcite, rutile and fluid (CO_2 etc.) inclusions

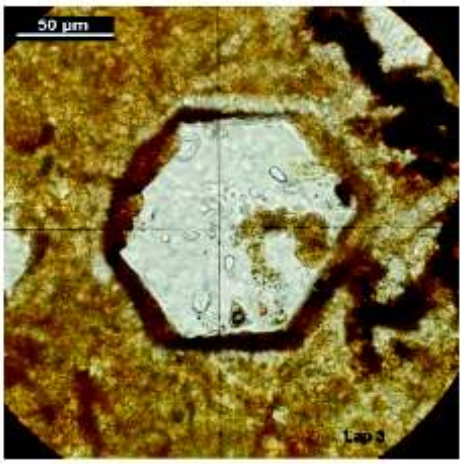

E Quartz with reaction rim; calcite and fluid (CO_2 etc.) inclusions

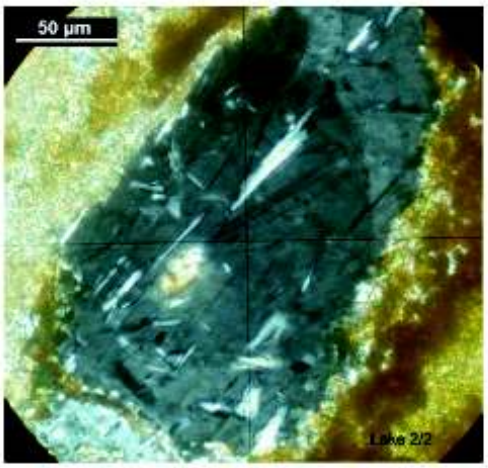

F Quartz fragment with muscovite inclusions

Plate VIII Scanning Electron Microscopy (SEM) images

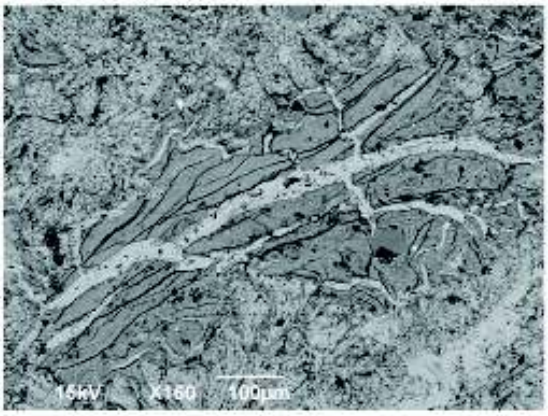

A Decomposed reddish glass shard cut by calcite veins in spinifex calcite matrix

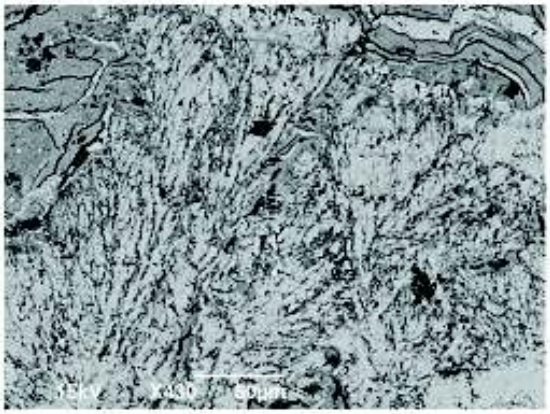

B Matrix of A: Spinifex calcite crystals

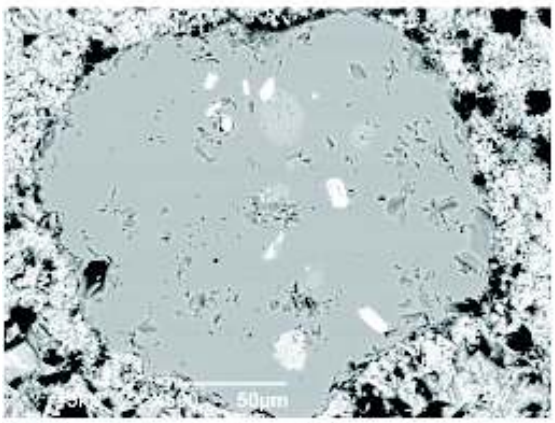

C Quartz in patchy spinifex calcite, inclusions: feldspar (grey), phlogopite (white), calcite/dolomite (irregular shape)

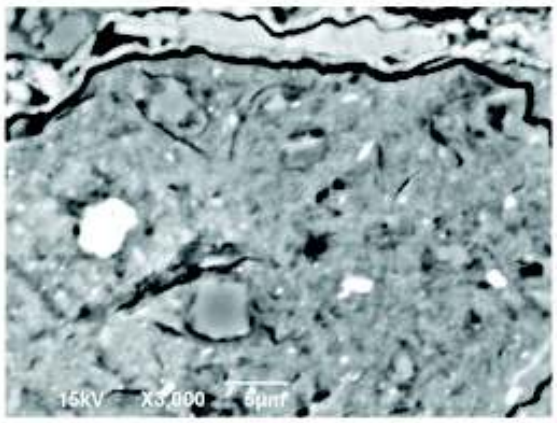

D Microcrystalline decomposed silicate glass; inclusions: quartz & calcite (grey), magnetite and ilmenite (white)

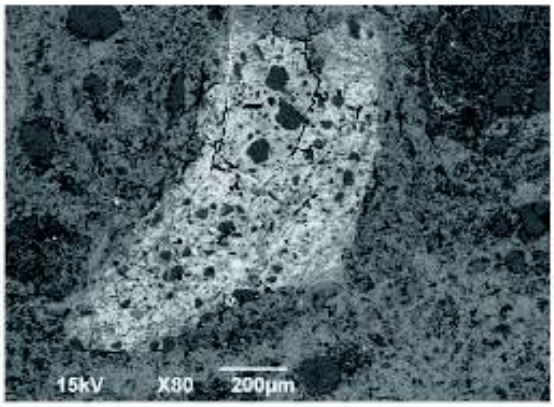

E Disintegrated magnetite/ilmenite fragment with quartz fragment inclusions in spinifex calcite matrix of impact breccia

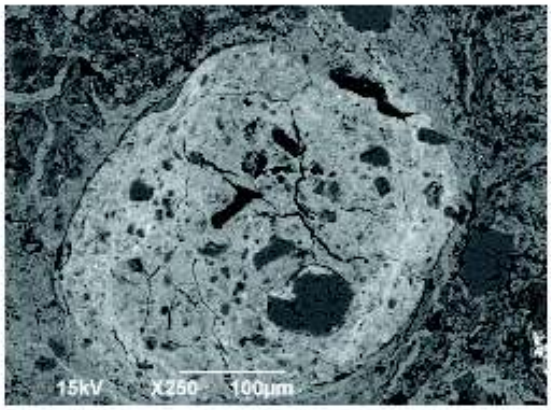

F Silikate spherule with concentric rims & microcystalline silicate core in spinifex calcite matrix: inclusions: Quartz, monazite

Plate IX Quartz disintegration in impact breccias

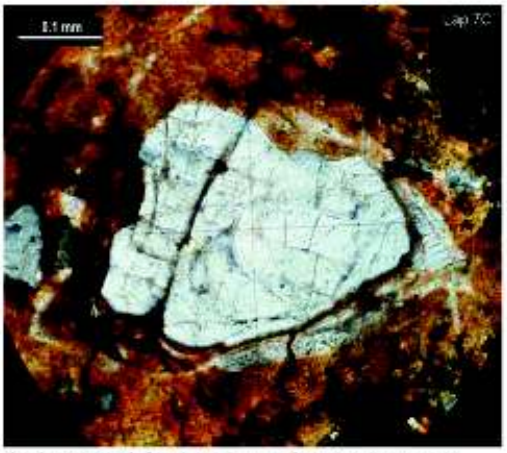

A Internal fracturing of quartz over-printing deformation lamellae

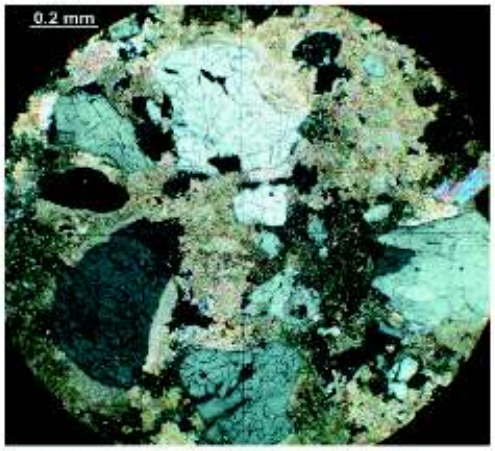

B Fractured quartz fragments in spherulitic impact breccia

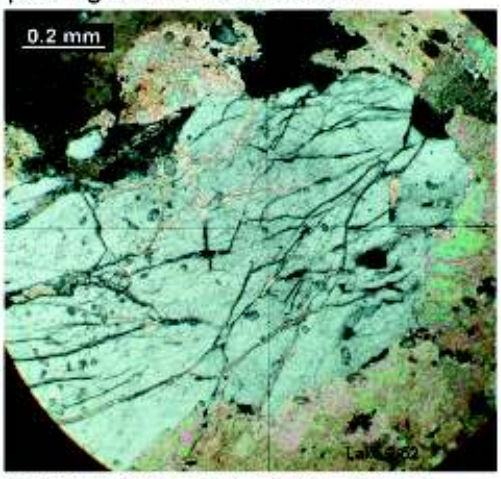

C Fractured quartz fragments in patchy spinifex calcite impact breccia

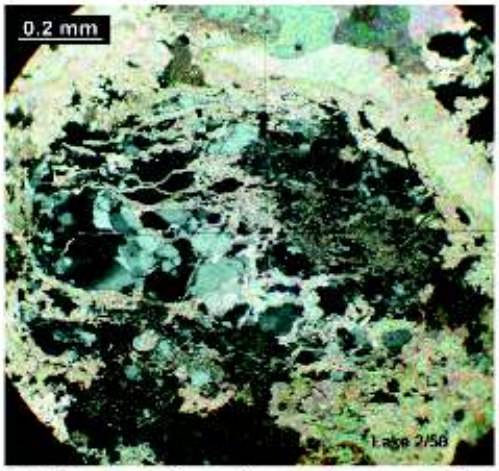

D Disintegration of mosaic quartz fragment in patchy spinifex calcite matrix

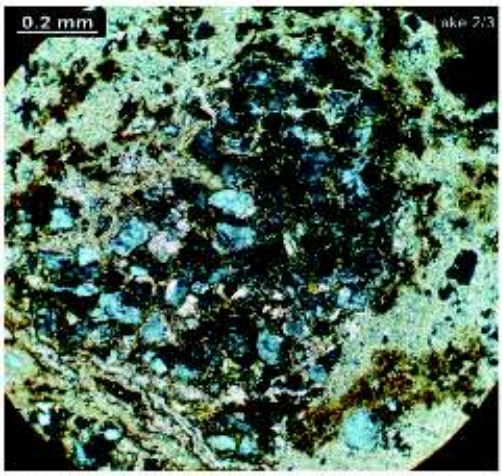

E Disintegration of mosaic quartz fragment in patchy spinifex calcite

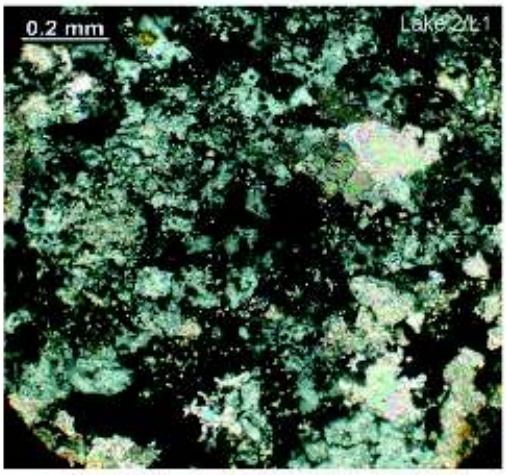

F Mosaic quartz spattered with tiny calcite and opake inclusions

2.3.6. Scanning Electron Microscopy (SEM) images, Plate VIII

Scanning Electron Microscopy (SEM) imaging was applied to study textures as well as chemical compositions of cryptocrystalline, microcrystalline groundmass, and minerals. Of particular interest are the compossitions of altered, “decomposed glass shards” , different generations of feathry spinifex calcite crystals, veins and groundmass matrices of globules and spherules. The compositions are given in Chapter 3.

2.3.7. Quartz disintegration in impact breccias, Plate IX

The fallback breccias consist of rock and mineral fragments, occasionally together with altered reddish flow-banded glass. In thin sections, mainly quartz and chert as well as subordinate shist fragments, which are frequently angular to sharp in outline, and their shapes indicate that they are broken clasts derived from the target rocks. Quartz fragments range in size from a few microns to millimeter and show often deformational effects from simple fracturing, planar fractures up to disintegration.

2.3.8. Planar fractures (PF) in quartz from impact breccias, Plate X

Planar microstructures in quartz and calcite (von Engelhardt & Stöffler 1965, Trepmann 2008, French & Koerberl 2010) can be used, however with caution, to identify shock-metamorphic events. Fracturing can be produced in quartz by both low-level tectonic deformation and low-pressure shock waves. In many cases, where the fractures are nonplanar and randomly oriented, the resulting fracture patterns are virtually identical, and their origin cannot be clearly interpreted as due to shock-deformational effects. Low-level shock waves (<10 GPa) can produce multiple sets of parallel open planar fractures (PFs) in quartz.

Small fragmental quartz grains of up to 100 micron are very abundant in the all fallback breccias, globules and spherules. In several cases, they show undulate extinction and Boehm lamellae, which are results of tectonic and metamorphic deformation in the crust during orogenic processes. However, in some cases “planar

fractures (PFs)" are also present. Real "planar deformation features (PDFs)" have not been found.

Plate X shows different features of more or less planar deformation. In some cases, the fracture plains are decorated with sets of tiny fluid inclusins.

Plate X Planar fractures (PF) in quartz from impact breccias

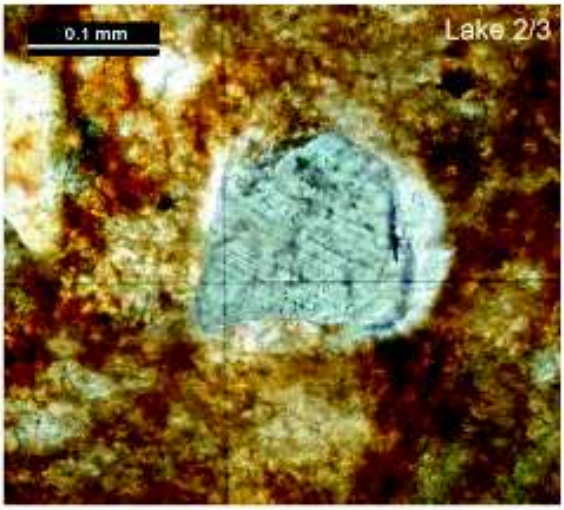

A Planar fractures in quartz

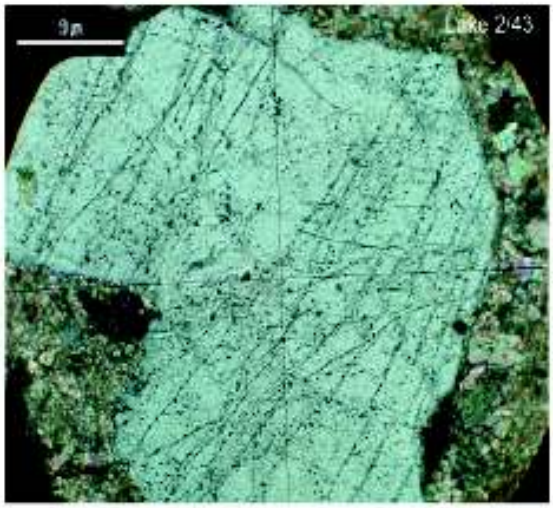

B Irregular to subparallel fractures as healed and decorated fracture plains

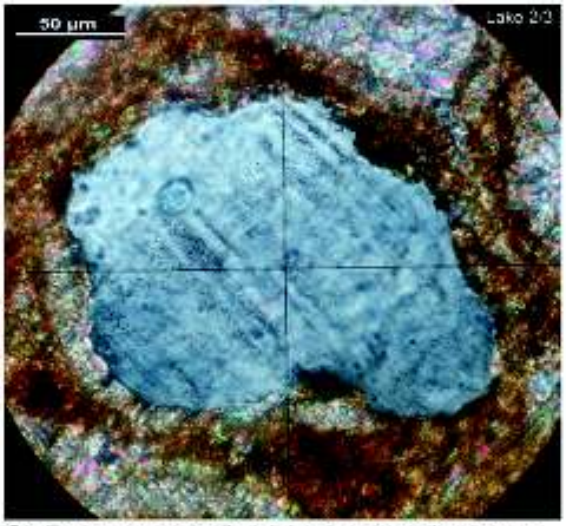

C Decorated (fluid inclusions) planar fractures in quartz spherule

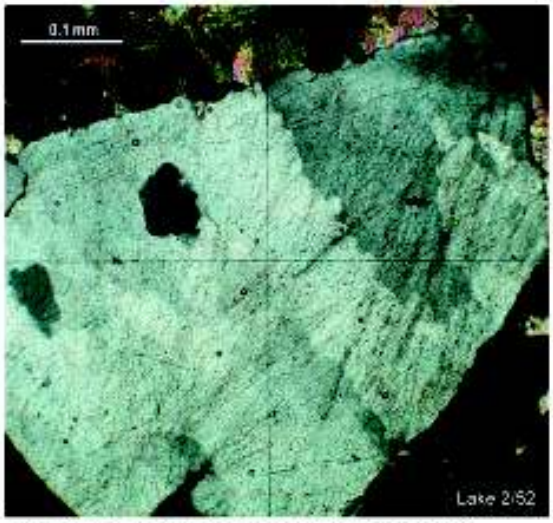

D Irregular to subparallel close fracture plains

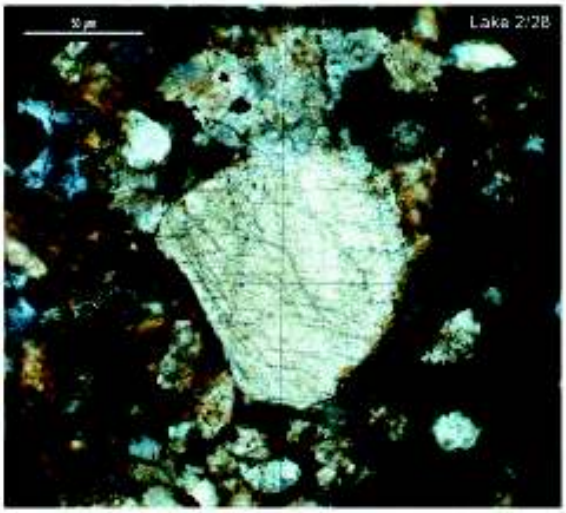

E Planar fracture plains in micro quartz fragment

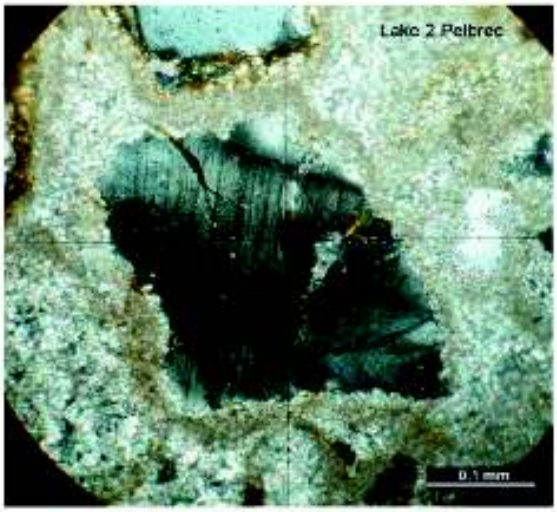

F Close-spaced fractures, possible metamorphic deformation lamellae

2.3.9. Special textural features in impact breccias, Plate XI

Several examples of special textural features in impact breccias, which are also results of shock-metamorphic events, are shown on Plate XI: (1) reaction and decomposition features of mineral and rock fragments within carbonatitic spherules and spinifex environment (Plate XI A, B & C). These two example show the irregular and disintegrated shapes of feldspars. In addition (B), disintegrated feldspar contains multiple sets of very small planar calcite lamellae; (2) altered and decomposed glassy fragments, which may exhibit relict melt compositions prior to recristallization. Such former glass shards might give the clue to understand the dynamic process and physical conditions of the shock-metamorphic effects during impact of the projectiles into the limestones, shales and cherts of the underground. Four pictures (C, D, E and F) demonstrate only the textural evidence of different "glassy relicts". Their chemical composition is given in Chapter 3.

2.3.10. Calcite crystallization sequence (veining) in impact breccias, Plate XII

Two different sets of veining can be distinguished within the clasts of the fallback impact breccias: (1) veins, with are mainly filled by feathery and euhedral quartz crystals with subordinate growth of idiomorph and irregular small patches of calcite. Such veins are restricted to clasts of dense radiolarian cherts. A typical example is shown in Plate XII A1 & B1; (2) carbonate veins, which occur throughout the entire fallback impact clasts. Typical examples are given in Plate XII A-F.

The relative sequence of calcite crystallization sequence in impact breccias is clearly expressed by veining textures. Calcite veining is a common feature in most carbonatitic clasts and occurs in all sizes from globules to clasts of several centimeters (Plate II A-D) . Euhedral calcite in different textural arrangements is the predominant phase in vein fillings, magnesium and iron bearing calcite and dolomite are subordinate. Exceptions are radial and concentric veins as well as cavity fillings in globular clasts (Plate II E&F, XII A-F).

Calcite crystallization sequence in XII A & B: Euhedral calcite in small euhedral crystals in irregular shaped and disseminated network of veins of (2), which

originated from the patchy spinifex matrix; (3) euhedral often coarse calcite with mosaic textures within late crosscutting set of veins. Their first stages are composed of magnesium and iron bearing calcite assemblages with microcrystalline and partly spinifex textures and are often associated with iron and manganese oxides (XII C, D, F; e.g. with psilomelane as in case XII E).

Plate XI Special textural features in impact breccias

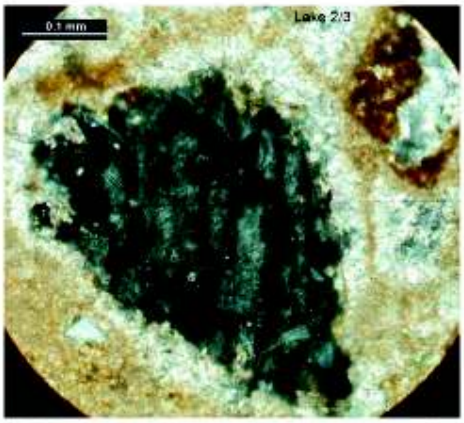

A Feldspar fragment with calcite reaction rim in sphelrulithic calcite matrix

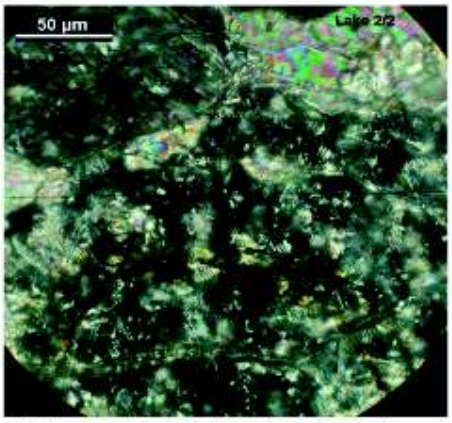

B Planar deformational features in euhedral calcite (polarized light)

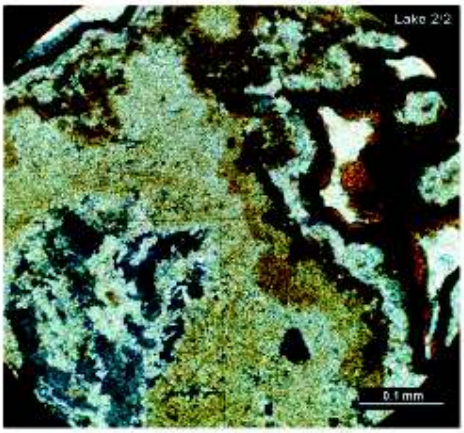

C Filigranic veining and fillings of carbonates and oxides in patchy spinifex

D Decomposed glass fragments in patchy spinifex calcite matrix

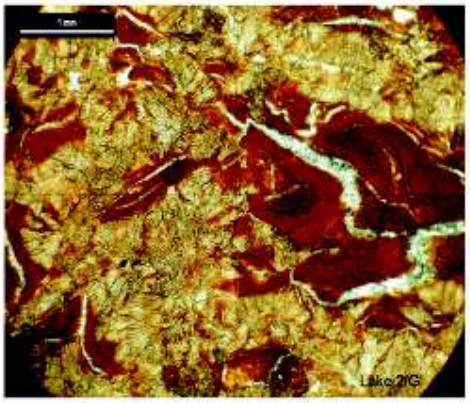

E Decomposed reddish glass fragments in spinifex calcite matrix

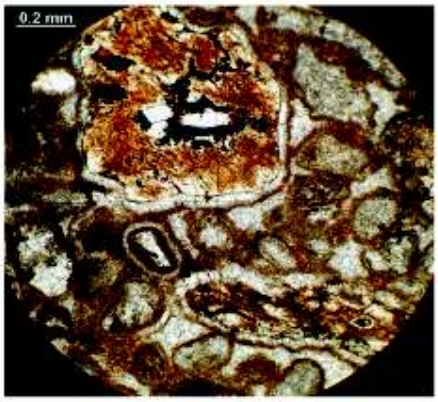

F Decomposed glass-spinifex clast in spherulitic breccia

Plate XII Calcite crystallization sequence (veining) in impact breccias

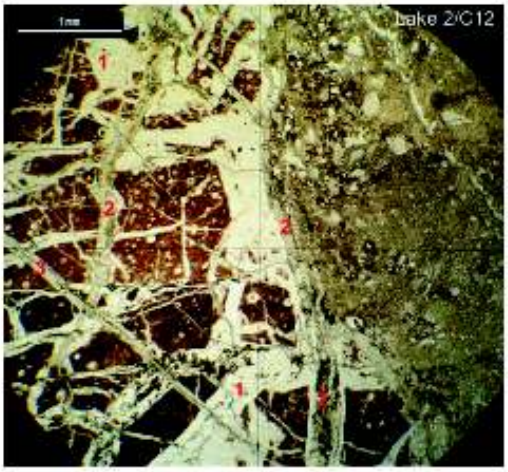

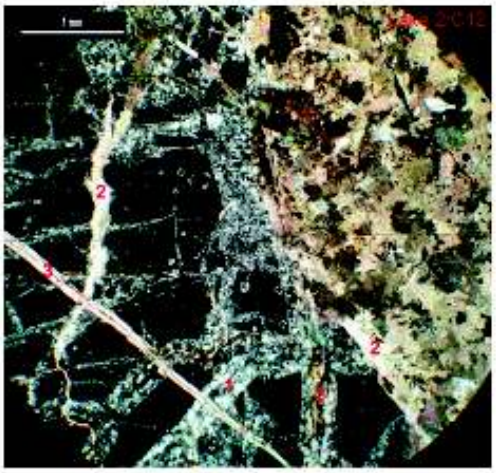

A & B (pol.light) Quartz-Calcite crystallization sequence between chert clast (left) and patchy spinifex matrix (right): 1 (quartz veins), 2 (syn-), 3 (post-spinifex calcite)

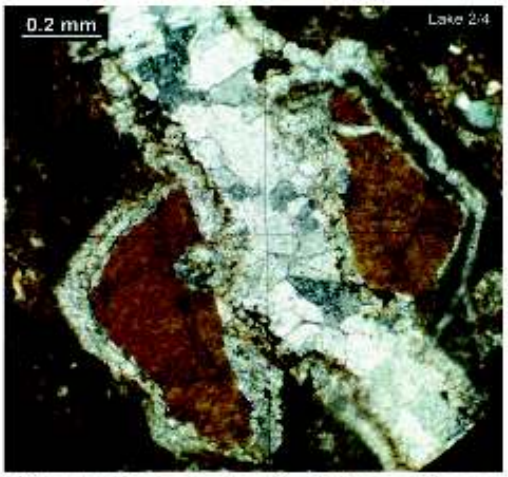

C Quartz (brown clast) - Calcite (3 generations, white) crystallization sequence

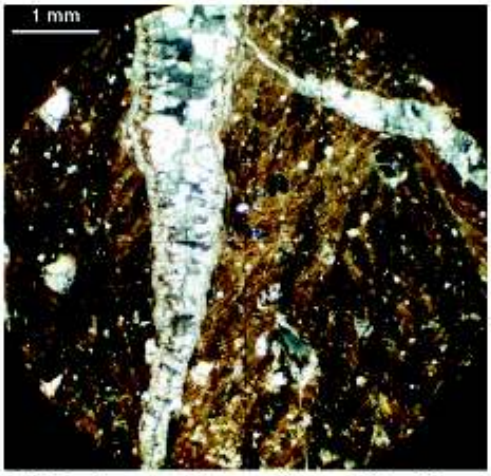

D Spinifex calcite - vein calcite (3 generations, white) crystallization sequence

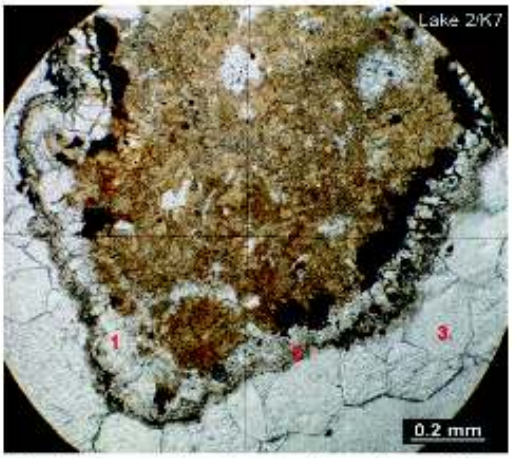

E Spinifex calcite (center) - vein calcite (3 generations,white,opakes) crystalliz.

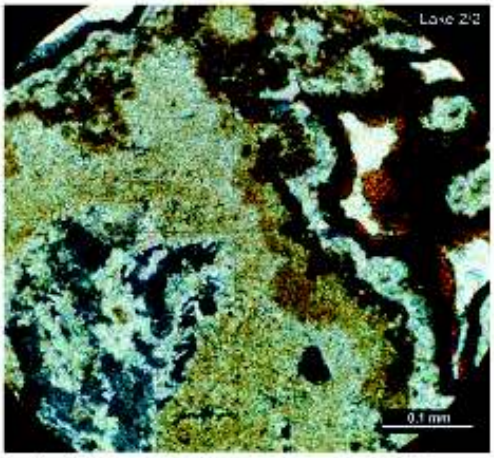

F Spinifex calcite - vein calcite (3 generations, white, brown) crystallization

Plate XIII Textures in impact breccias worldwide

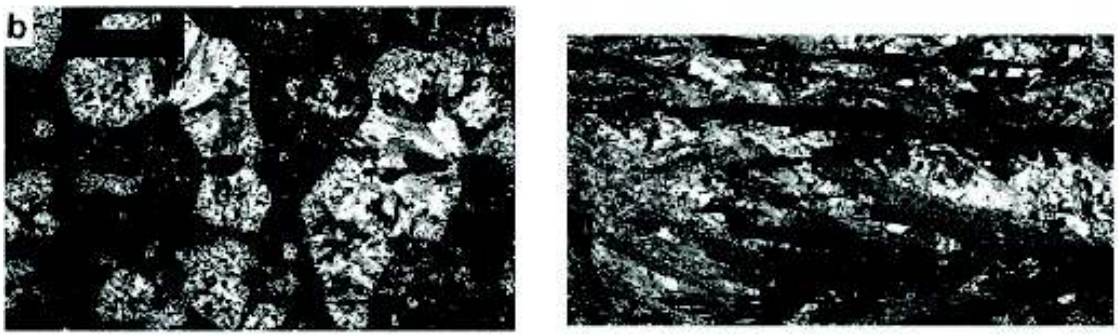

Quench spinifex textures of calcite crystals inside globules in silicate glass (black). Nördlinger Ries Miocene impact crater. Scale bar is 0.77 mm (Graup, 1999).

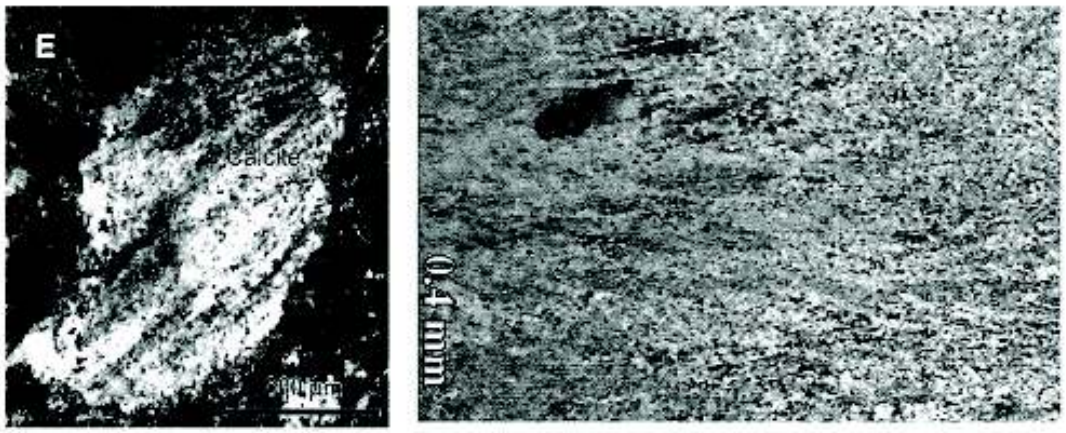

Feathery spinifex calcite from breccia Chicxulub K-T impact. Jones et. al. (2000)

Feathery spinifex calcite in impact breccia Devonian Alamo crater, Nevada. (Pinto & Warme 2008)

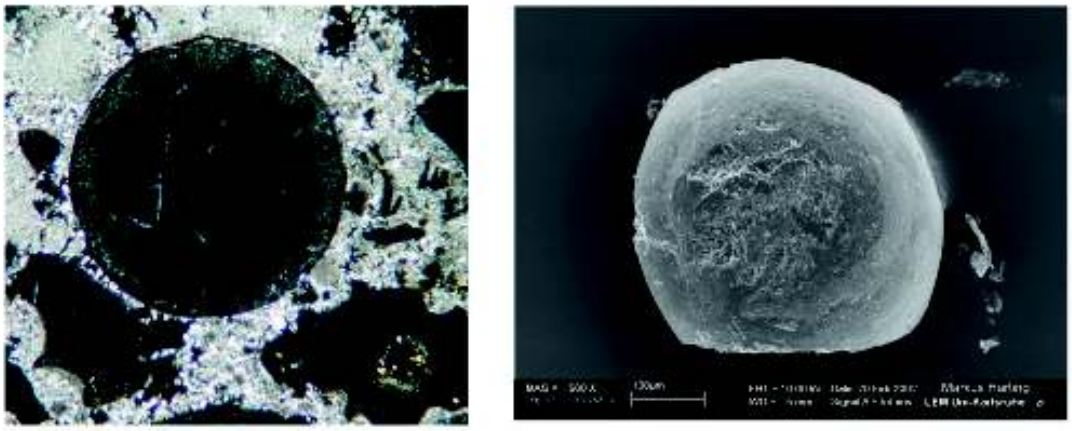

Thin-section of Spherule-bearing sediment and Scanning Electron Microscope picture (NE-Mexico) related to Chicxulub K-T impact. M. Hartung (2002)

2.3.11. Textures in impact breccias worldwide, Plate XIII

The conditions of impact produce an unusual group of melted, shocked, and brecciated rocks, some of which fill the resulting crater, and others which are transported, in some cases to considerable distances from the source crater. Only the presence of diagnostic shock-metamorphic effects and, in some cases, the discovery of meteorites, or traces thereof, is generally accepted as unambiguous evidence for an impact origin.

Examples of carbonate textures from impact breccias from well established impact craters worldwide should demonstrate the textural similarities to the carbonatitic backfall breccia of the Zerelia impact crater lakes. All textural and chemical criteria for the recognition of impact melts derived from sedimentary rocks are summarized by Osinski et al. (2008).

Plate XIII contains calcite spinifex textures and spherules of three large most typical, well established meteorite craters: (1) the Miocene Nördlinger Ries Crater in Germany (von Engelhardt & Stöffler 1965 and 1968, Graup 1999); (2) the huge Chixulub impact crater in the Gulf of Mexico at the Cretaceous/Tertiary boundary, which led to the extinction of dinosaurs (Alvarez et al. 1980 &1995, Alvarez 1997, Hartung 2006), and (3) the Devonian Alamo crater, Nevada (Pinto & Warme 2008).

In addition, a critical review on shock-deformation effects is given by French & Koeberl (2010).

Shock deformation can be expressed in microscopic forms (e.g., distinctive planar deformation features (PFs and PDFs) in quartz.

CHAPTER 3

MINERAL AND ROCK CHEMISTRY

Chemical studies on minerals and rocks from impact breccias at several impact craters within sedimentary environments (e.g. Nördlinger Ries and Haughton crater) made clear that calcite diplaying spinifex, globule and spherulitic textures indicative of an impact melt origin is also distinctly different in chemical composition than carbonates from the original target carbonate rocks and their postimpact hydrothermal alteration effects (Osinski et al. 1995, Koeberl & Henkel (eds.) 2005). Especially, the post-shock-metamorphiphic networks and late undeformed calcite veins fallback breccias indicate the existence of hydrothermal overprinting immediately during and after the impact but prior to their deposition from the Zerelia craters.

3.1. MINERAL CHEMISTRY

The major mineral species in the Zerelia fallback carbonatitic samples were identified by optical microscopy in thin section of 10 to 20 micron thickness, X-ray diffraction (XRD), and scanning electron microscopy (SEM) and Raman spectroscopy.

Chemical qualitative as well as quantitative elemental abundances were determined for some SEM samples by energy-dispersive X-ray dispersive spectrometry (EDS). Major crystalline phases are calcite, iron and magnesium bearing calcite, quartz, dolomite and clay minerals. Minor minerals species include the iron oxides (FeOOH), manganocalcite (Ca, Mn)CO_3 psilomelane $Ba(Mn^{2+)(}Mn^{4+})_8O_{16}(OH)_4$, ilmenite ($FeTiO_3$), rutile ($TiO_2$), apatite ($Ca_5(PO_4)_3F$), baumite $(Mg,Mn,Fe,Zn)_3(Si,Al)_2O_5(OH)_4$, magnetite ($Fe_3O_4$)and chromite as well as alkali feldspar, micas, antigorite, and olivine $(MgFe)_2SiO_4$. Decarbonated microbreccia samples showed the ambiguous existence of periclase (MgO) and Millerit (NiS).

3.2. ROCK CHEMISTRY

Chemical composition of cryptocrystallin, microcrystallin matrices as well as of altered, devitrified reddish glass fragments in spinifex calcite matrix in a typical microbreccia carbonatitic rock clast is given in Table 1, the matrix compositions of several globule in Table 2. All these compositions may represent mixtures of cryptocrystalline mineral phases and do not match at all any known magmatic melt.

Table 1

Chemical composition of cryptocrystallin, microcrystallin matrices as well as of altered, devitrified reddish glass fragments in spinifex calcite matrix in a typical microbreccia carbonatitic rock clast (see sample G in Plate II C and Plate XI E). Analytical procedures: Energy dispersive X-ray spectrometer (EDS) at a JEOL Scanning Electron Microscope.

Oxides wt. %	Sample G grey matrix	Sample G reddish "glass" shards 5 points	Sample G mixture spin. Cct-clay	Sample G spherulitic matrix 5 spots
SiO_2	78.81	50-52	35.13	41-45
TiO_2	nd	0.3-0.9	0.29	0.25-0.4
Al_2O_3	12.84	29-32	20.10	24-29
FeO	6.35	9-11	7.72	19-25
MgO	1.03	1.8-2.1	2.02	0.9-1.2
CaO	nd	2.2-2.4	32.49	2.7-4.5
K_2O	0.97	2.6-2.8	2.17	1.8-2.6
Total	norm.100	norm.100	norm.100	norm.100

Table 2

Chemical composition of cryptocrystallin and microcrystallin matrices in several globules (see Plate IV and VIII)

Oxides wt. %	Globule 5A1	Globule 5B4	Globule 5B6	Globule 5D3	Globule 5E4	Globule 5E1	Globule 3A1
SiO_2	91.04	54.93	56.55	34.39	8.20	9.90	11.04
TiO_2	nd	nd	nd	0.14	nd	nd	nd
Al_2O_3	4.18	23.22	27.03	11.02	3.69	4.48	5.61
FeO	3.60	13.85	9.35	7.80	2.29	1.73	nd
MnO	nd	nd	nd	11.03	nd	nd	64.55
MgO	nd	1.61	1.85	1.17	0.89	1.22	0.95
CaO	nd	2.41	1.32	29.84	83.96	72.65	2.22
Na_2O	nd	nd	nd	0.57	nd	0.80	nd
K_2O	1.18	2.39	2.19	1.56	0.32	0.62	1.02
F	-	-	-	-	-	7.27	-
SO_3	-	-	1.60	-	0.50	0.50	0.47
Y_2O_3	-	-	-	-	0.16	0.82	-
BaO	-	-	-	0.91	-	-	13.85
Total	norm.100	norm.100	norm.100	norm.100	norm.100	norm.100	norm.100

The relative high Al_2O_3 and SiO_2 abundances in some globules seem to be anomalous. They do not represent analytical problems, since the have been found also in other impact carbonatites (Osinski et al. 1995). Experiments have shown, that rapid crystallization (quenching)of high-temperature SiO_2 carbonate melt can produce SiO_2-rich carbonatites (Brooker 1998).

Several clasts with relatively homogeneous fine-grained and feathery to spinifex calcite groundmass were analyzed with XRF method to obtain their bulk chemical composition. The major elements show a rather marly limestone composition with SiO_2 30-35 wt.%, CaO 28-32 wt.%, Al_2O_3 5-6 wt.%, K_2O 0.6-0.7 wt.%, TiO_2 0.35-0.45 wt.% and a low MgO 0.6-0.9 wt.%. The trace elements display rather low concentrations: Rb 25-35 ppm, Sr 35-65 ppm, Ba 130-400 ppm, Nb 5-6 ppm, low values of Light Rare Earth Elements (LREE); Cr 110-160 ppm, Ni 50-65 ppm and Zn 40-50 ppm. The only unusual enrichment exists in Y with 30-70 ppm. Such a composition supports an origin of these clasts from marly limestones, but differs dramatically from the composition of

carbonatitic globules from volcanic diatremes in the ultra-alkaline Province north of Rome (Stoppa & Lupini 1993).

3.3 CONCLUSION

The petrographic and chemical evidence of the collected fine-breccias and pebbles leads to the interpretation of the material as "impact fall back breccias and carbonatitic tectites due to meteoritic impact, although up to now no meteorite fragments have been found. According to the size of the crater lakes the dimensions of the meteorite, which might have split into two fragments, should have been about 10-30 m before reaching the surface. The temperature and pressure of the impact may have been sufficient to decompose and melt the limestones followed by quenching during cooling and decompression to form the carbonatitic pebbles and spherules.

Analytical procedures

The Institute of Geochemnistry and Petrology operates the following analytical instruments, most of them the latest generation.

JSM-6510LA Analytical Scanning Microscope

JEOL JSM-6510A is a high-performance, scanning electron microscope for fast characterization and imaging of fine structures. JSM-6510 enables observation and analysis in rock thin sections of 27 x 47 mm size.

With a high resolution of 3.0nm at 30kV, the JSM-6510A delivers amazing clarity of the finest structures. In addition to routine imaging at several hundreds of times greater resolution than the optical microscope, and with a focal depth several tens of times greater than the optical microscope, the SEM allows for detailed measurements. An optional energy dispersive X-ray spectrometer (EDS) provides elemental analysis.

Raman Spectroscopy

The micro-Raman spectrometer is a DILOR Labram istrument equipped with an Olympus mcroscope an internal He-Ne laser and an external Ar-ion laser.. Three exciting wavelength are available: 488 nm, 514.5 nm, 632 nm. Currently we run the instrument at 514.5 nm.

Micro-Raman spectroscopy allows the identification of mineral species, liquids and gas species in fluid inclusions at a micrometer-scale resolution. No special sample preparation is required except for the fluid inclusions analysis.

X-ray Powder Diffraction (XRD)

Powder X-ray Diffractometer (Bruker, AXS D8 Advance), equipped with a Lynxeye superspeed detector and an automatic sample changer for 9 samples for the identification of mineral species.

X-ray Fluorescence Analysis (XRF)

Wave-length dispersive X-ray fluorescence spectrometer (WD-XRF, Axios, PANalytical), equipped with 5 diffraction crystals for bulk chemical analysis of rocks. Standard analyses are performed on fused glass-beads prepared from rock powder mixed with Lithium-Tetraborate (1:5 mixture) using a Claisse M4® fluxer. A minimum of 1 gram of fired rock powder is required.

The current setup includes 10 major (SiO2, TiO2, Al2O3, Fe2O3, MnO, MgO, CaO, Na2O, K2O, P2O5) and 21 trace elements (S, Sc, V, Cr, Co, Ni, Cu, Zn, Ga, Rb, Sr, Y, Zr, Nb, Ba, La, Ce, Nd, Pb, Th, U). The calibration bases on ca. 30 certified international standards with emphasize on igneous and metamorphic rock compositions. However, for the case of bulk analysis of the Zerelia carbonatitic breccias, a calibration for sedimentary (mainly carbonate) rocks was used.

CHAPTER 4

GEOPHYSICAL SURVEYS

4.1 GRAVITY MEASUREMENTS

A gravity survey was carried out in the area around the two lakes (Fig. 4.1) to form the Gravity Anomaly Field. About 80 gravity measurements were taken by the use of the LaCoste & Romberg G-496 gravity meter. The gravity measurements were taken at a spacing of about 100-150 meters at an effort to cover satisfactorily all area around the two lakes.

Figure 4.1 General view of the Almyros twin lakes

For the height control, the nearby pillar of the Hellenic Military Service (HMS) provided the coordinates, not only in the vertical, but also in the horizontal. A geodetic GPS receiver of LEICA (type AX1202) was mounted on top of the pillar, and served as a base station (particularly for the vertical component) for the kinematic GPS survey for coordinate determination of the gravity stations, recording every 5 secs (Fig. 4.2). The rover GPS station was of the LEICA type SR299, which was recording for a period of 3-4 min above every gravity station to determine basically

the height with an accuracy of better than 1-2 cm, even though the accuracy in the horizontal coordinates was much higher (<1 cm).

Figure 4.2 Outline of the GPS Base station (on the pillar) together with the location of the Gravity Base station.

A gravity base station was established nearby the HMS pillar, where a repeat measurement was performed every 3-4 hour for control of the gravity meter drift. The field gravity base station was tied up to the Athens University IGSN'71 absolute value gravity station (Hipkin et al., 1988).

The gravity measurements were reduced to gravity anomaly values, where terrain corrections were performed at a distance of about 22 km around each station. Therefore, all gravity values of our gravity survey are referred to IGSN'71, based on the Gravity Reference Formula of 1967 (GRF'67). All the reduced values of the gravity stations are presented in Appendix 1.

The Gravity Anomaly Map of the area is presented in Figure 4.3a & b. It was found that a surface density of about 2 gr/cm^3 was appropriate to reduce the gravity anomaly values after fitting a 2nd and 3rd polynomial fit to the observed gravity anomaly field.

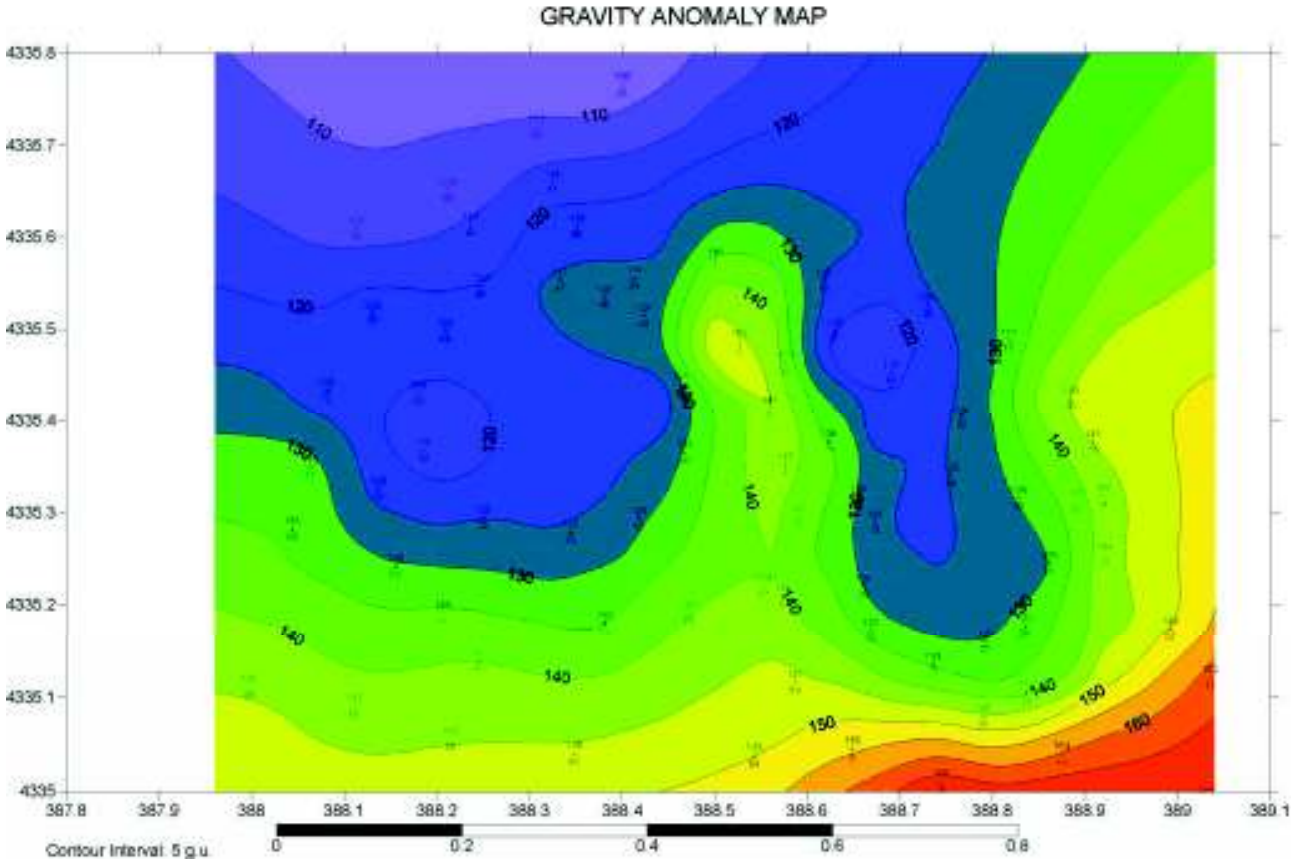

Figure 4.3a. Gravity Anomaly Map, referred to IGSN'71 and GRF'67 with gravity stations.

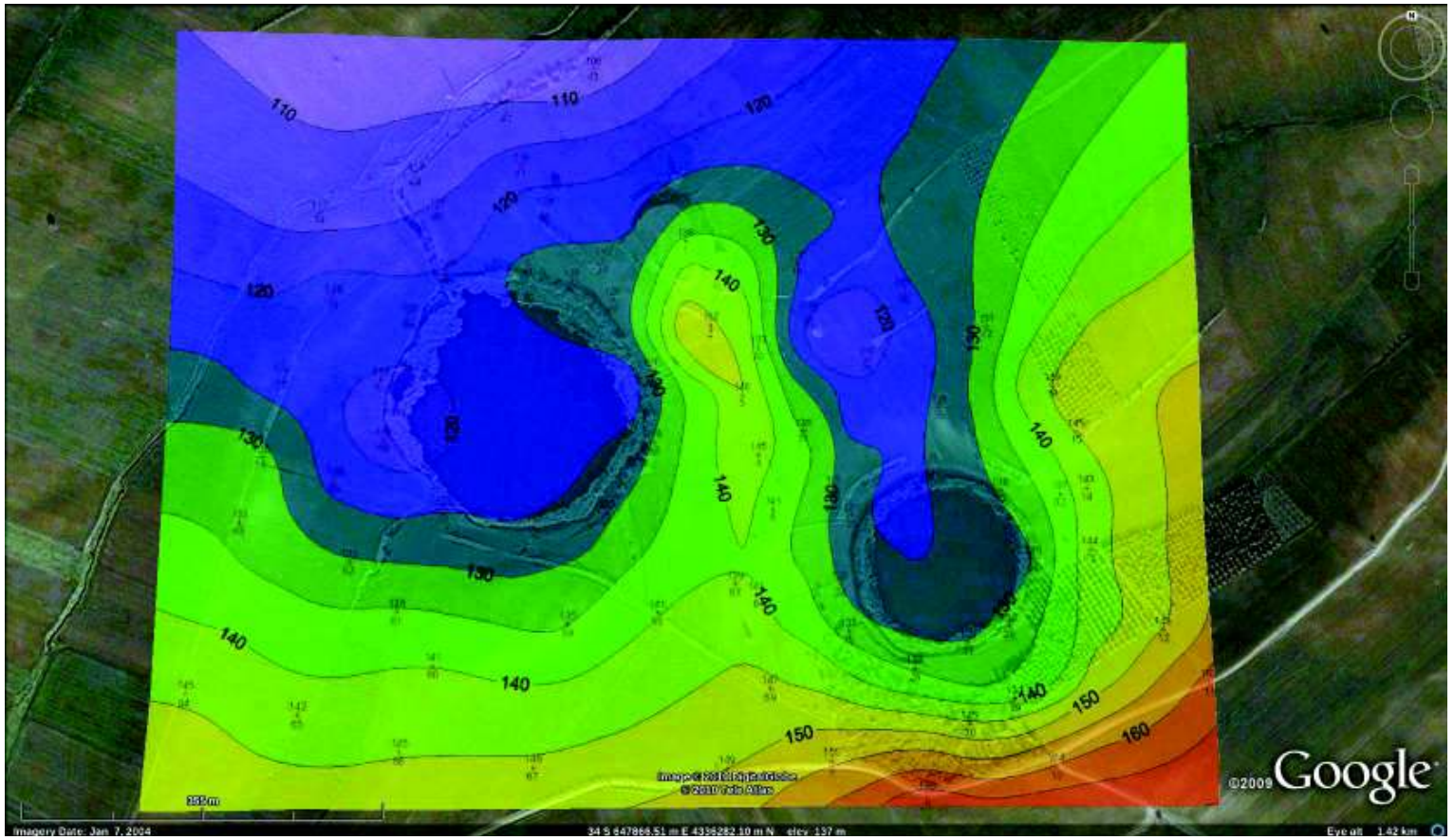

Figure 4.3b Gravity Anomaly Map superimposed on the Google satellite image, referred to IGSN'71 and GRF'67.

It can be seen that two gravity lows are associated with the localities of the two lakes, reaching values of about 120 gravity units (gu).

These gravity lows are more distinct at the Residual gravity anomaly map (Fig. 4.4) that was formed for modeling attempts. It was resulted after subtracting a linear regional trend of about 50 gu/km. The regional gravity anomaly map of the broader area was also taken into consideration for the previous estimation of the regional trend.

These two residual gravity anomaly lows have values at about -10 gu. Referring to their horizontal lateral extent, it appears that the one associated with the western lake (which is the largest one) is larger compared to the eastern one over the smaller dimensions lake, which is also elongated of N-S direction, narrowing to the north.

Four (4) profiles were constructed (Fig.4.4), two of E-W direction, and another two of N-S direction for modelling purposes. The inversion tomography of the density contrast results along these four residual gravity profiles may be seen in figures 4.5a, 4.5b, 4.5c & 4.5d.

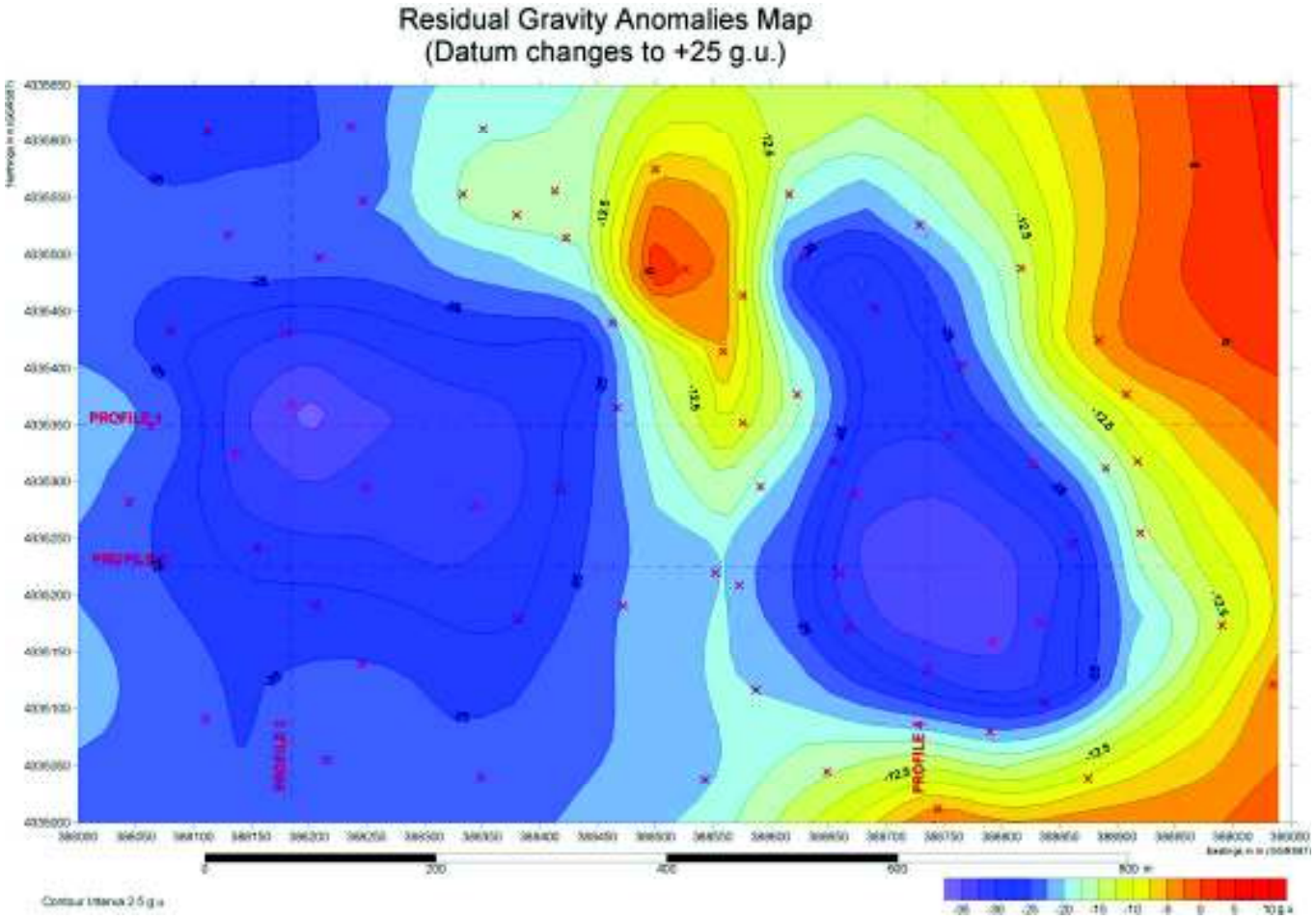

Figure 4.4a. Residual Gravity Anomaly Map showing the directions of the four profiles for modelling. The two lakes are marked as dashed circles.

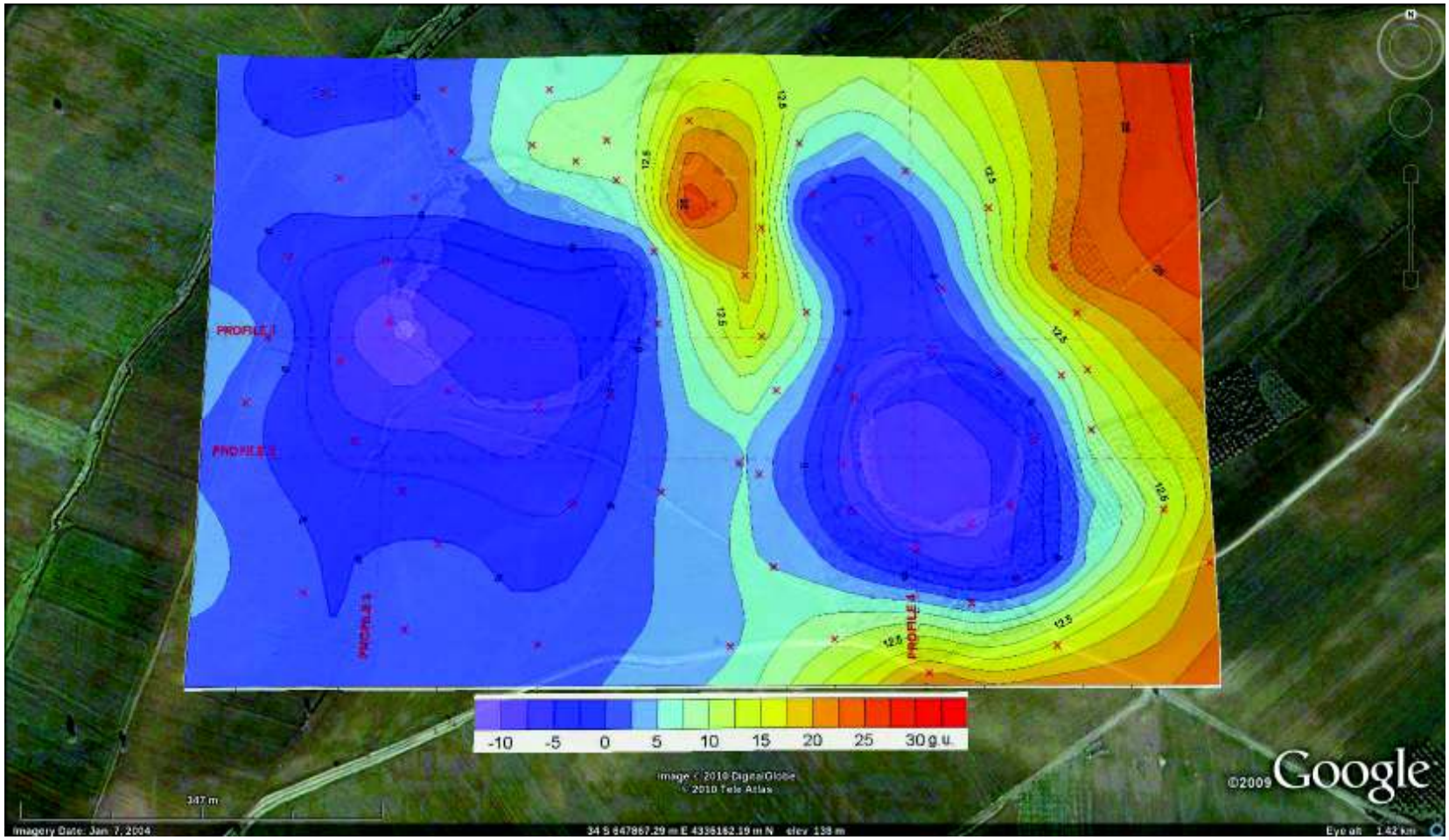

Figure 4.4b. Residual Gravity Anomaly Map superimposed on a Google satellite image

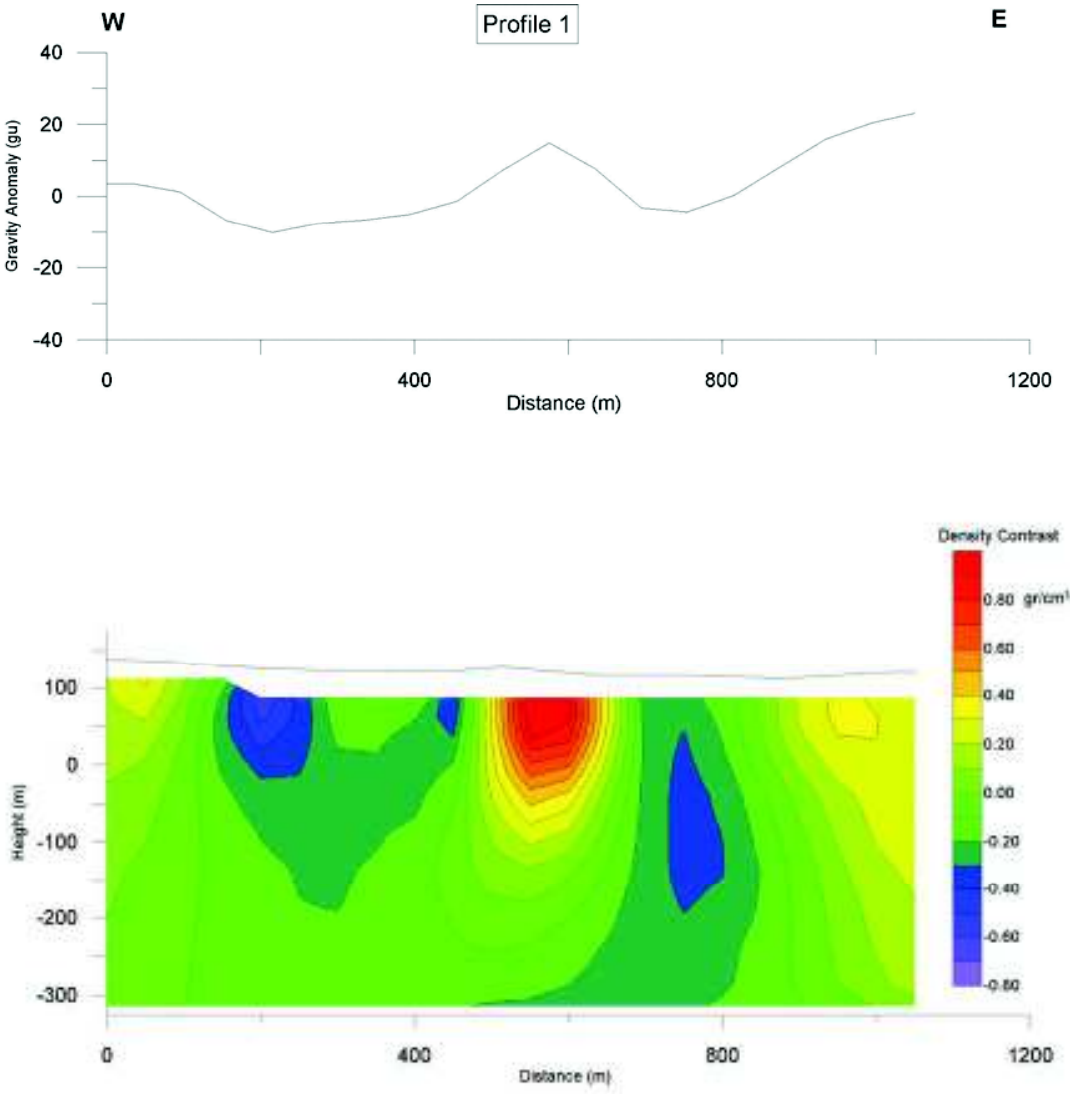

Figure 4.5a. Modelling of the Residual Gravity Profile 1.

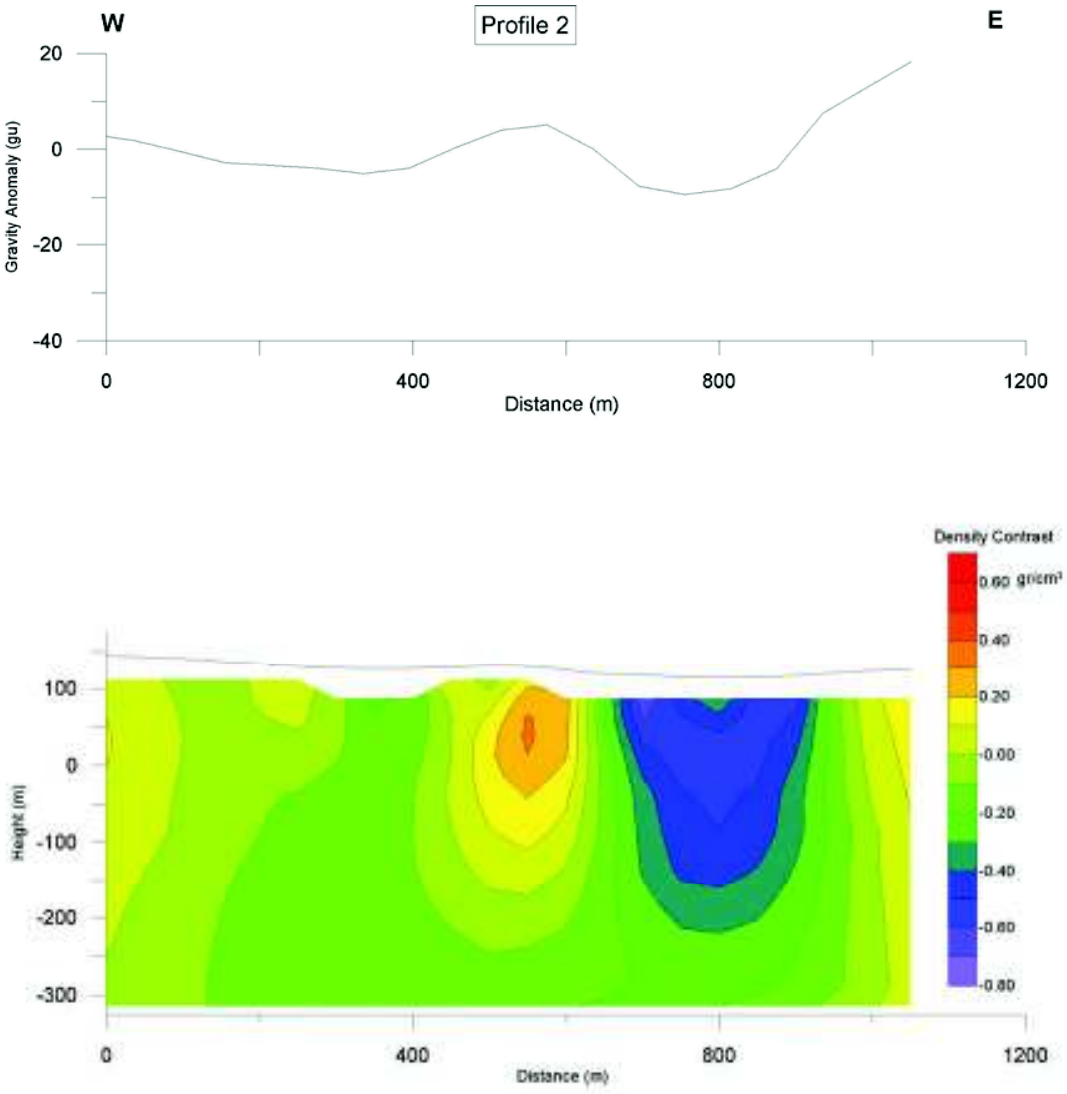

Figure 4.5b. Modelling of the Residual Gravity Profile 2.

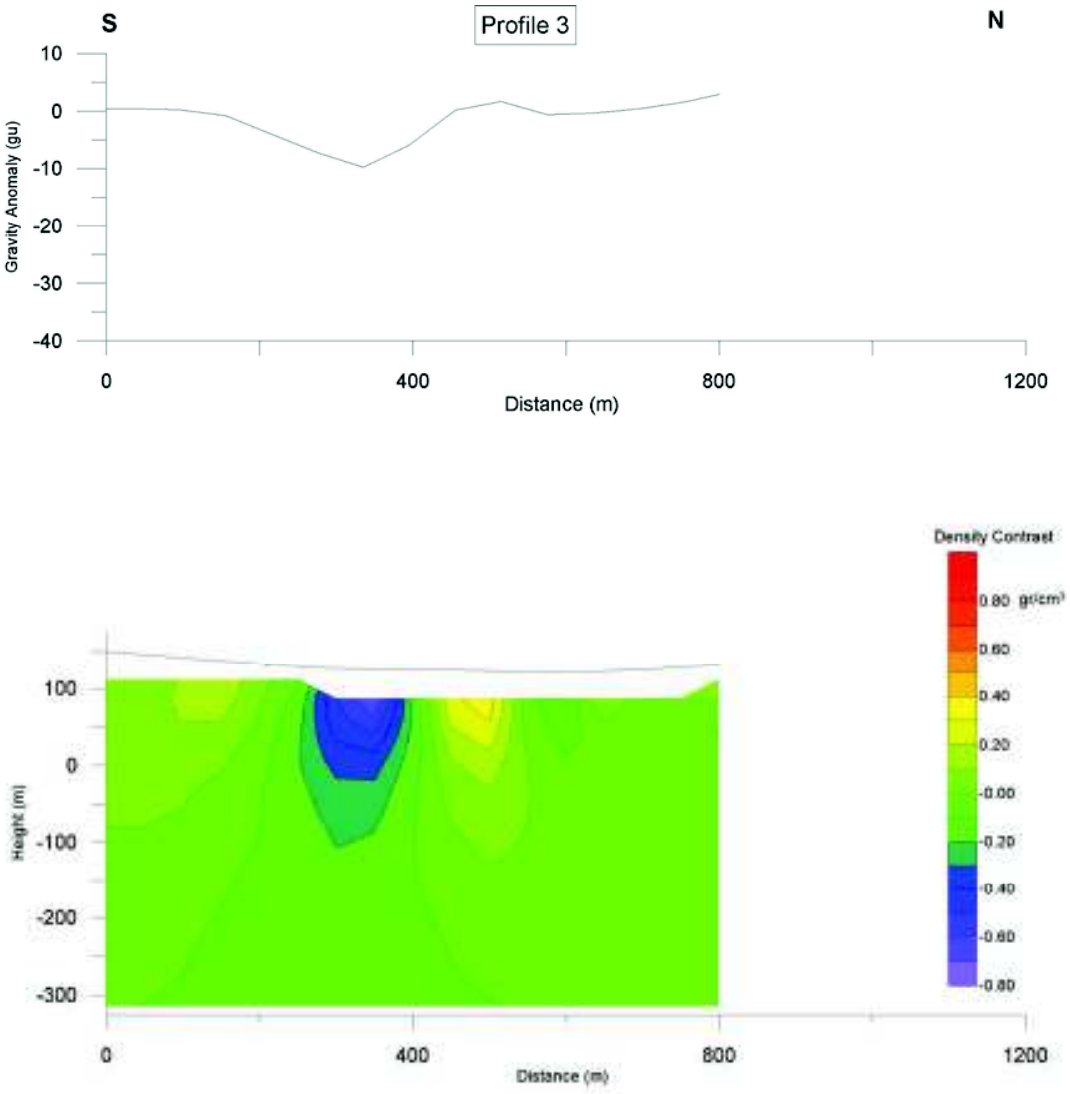

Figure 4.5c. Modelling of the Residual Gravity Profile 3.

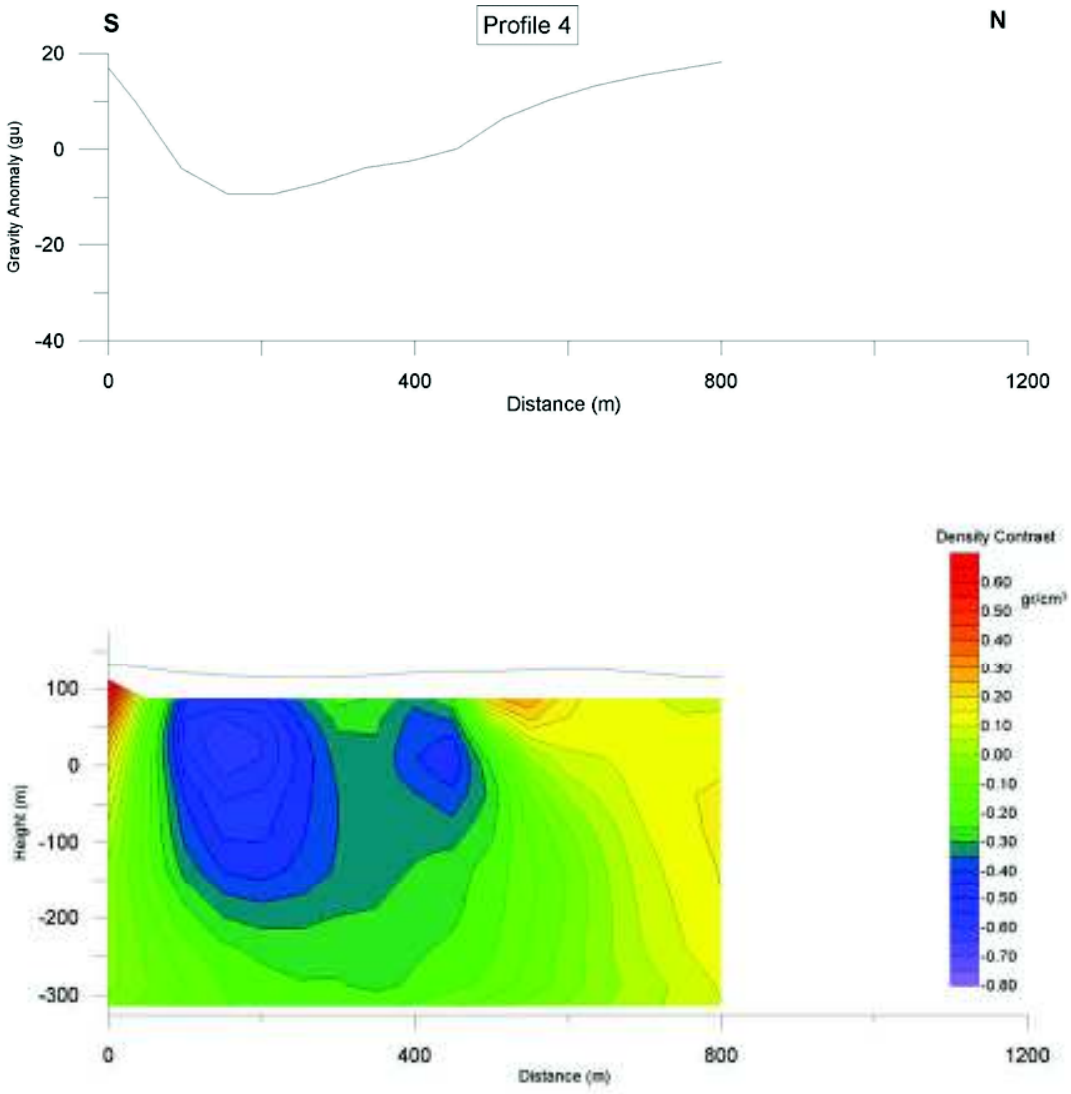

Figure 4.5d. Modelling of the Residual Gravity Profile 4.

Gravity anomalies in impact structures may result from quite different processes. Small, simple craters in general show a roughly circular negative anomaly, as actually happens in our case in this study. The mass deficit is due here to the usually low-density breccias the crater floor, post-impact young crater sediments, and fracturing of the rocks beneath and around the crater. Like in simple craters, rock fracturing and low-density impact melt rocks, suevites and other breccias cause negative anomalies, and post-impact crater sediments may also contrast with the pre-impact target rocks. In addition, relatively positive anomalies are measured, if rocks of higher density

were uplifted in the modification stage of the cratering process forming uplifts and rings. Shock lithification of porous rocks may also lead to locally increased density.

In this context, gravity measurements prove to be a valuable tool in the investigation of impact structures. They are important to detect buried impact structures, as for example the famous giant Chicxulub structure (Fugugauchi, 1993), and they can trace the original size of deeply eroded craters where only relics of impactites indicate an impact origin, as for example the Rochechouart impact structure (Vermeesch et al, 2004).

It is observed that along profiles 1 and 3 (Fig. 4.4b), the areal extent of the western gravity anomaly (over the largest lake) was modelled, showing a small graben-type feature in a form of a crater, extending at depths up to 200-250 m, as depicted by the density contrast tomography (Fig. 4.5a & 4.5c). Considering Profiles 2 and 4 (Fig.4.4b), almost the same crater feature was also modelled for the eastern residual gravity anomaly over the eastern lake. The density contrast tomography (Fig. 4.5b & 4.5d) indicates a crater extending at about a depth of 200-300m. The form and shape of the above negative gravity anomalies are consistent with those in other areas of the world, where meteorite impacts occurred, as the Steinheim impact (Ernstson, 1984), and elsewhere (eg. Bottke et al. 2007).

References

Bottke, W. F., Vokrouhlicky, D., and Nesvorny, D. (2007). An asteroid breakup 160 Myr ago as the probable source of the K/T impactor. *Nature* 449 , 48-53.

Ernstson, K. 1984, A gravity-derived model for the Steinheim impact structure. - *Int. J. Earth Sci*., 73/2, 483-498.

Fucugauchi (1993), Chicxulub multiring impact basin: size and other characteristics derived from gravity analysis, Science, 261, 1564- 1567.

Hipkin, R.G., Lagios, E., Lyness, D., & Jones, P. (1988). Reference gravity stations on the IGSN'71 standard in Britain and Greece. *Geophysical Journal Intern*., 92, 143-148.

Vermeesch, Peggy M. and Morgan, Joanna V. (2004). Chicxulub central crater structure: Initial results from physical property measurements and combined velocity and gravity modeling. *Meteoritics & Planetary Science*,39 (7),1019-1034.

4.2 MAGNETIC MEASUREMENTS

Total field magnetic measurements were conducted (Fig. 4.6) in the same survey area to determine the Total Magnetic Field at an effort to detect magnetic anomalies relating to the probable presence of a magnetic body supporting the meteorite impact hypothesis.

Total field magnetic readings were performed using total field magnetometers of the GEOMETRICS G-856 type along 12 profiles at a spacing of 10 m. Magnetic measurements were also taken peripherally around the two lakes as indicated in figure 4.6. More than 400 readings were taken for a period of two days during which a base magnetometer was continuously recording at a nearby site every 1 sec to form the daily variation of the local magnetic field. The coordinates at each station were determined by the use of a Magellan GPS receiver with an accuracy of better than 2-3 meters.

Figure 4.6. Photos from Magnetic Measurements Fieldwork

Corrections for the normal field and the diurnal variation were made to form the magnetic anomaly value for each station. The Total Field Magnetic Anomaly Map was constructed from all stations shown in figure 4.7, while all magnetic values are listed in Appendix 2.

As can be seen from the magnetic anomaly map, the eastern part of the area, as well as the half northern and southern part is is characterized by positive anomalies, which should be attributed to the basement geological formations. The same positive feature extending N-S is the ridge separating the two lakes, forming actually a part of the basement.

The two lakes are also associated with two magnetic anomalies. The eastern lake is dominated by a large negative magnetic anomaly encompassing even a region outside the lake. There is also another positive anomaly at its eastern flank, but this should rather be attributed to as part of basement characteristics. Magnetic readings have not been taken on the surface of the two lakes, so the values over them have been produced by the interpolation routine.

The situation on the western lake is almost the same. A negative anomaly dominates all of its southern flank which swings to the west along its western part. However, most the lake is covered by positive anomaly values that have to be treated with caution since they are deduced by interpolation. Therefore, the magnetic anomaly map should only qualitatively be considered. However, the higher magnetic values at the margins of both lakes corresponding to higher susceptibility values are consistent with the case of the Chiemgau meteorite impact in Bavaria (Ernstson 2010). Also the negative magnetic anomalies prevailing over most of the horizontal extent of both lakes are consistent with the Azuara impact in Spain (Ernstson & Fiebag, 1992). Similar case studies may also be found by the reader in the following site: http://www.impact-structures.com/geophysic/gravity_surveys.html

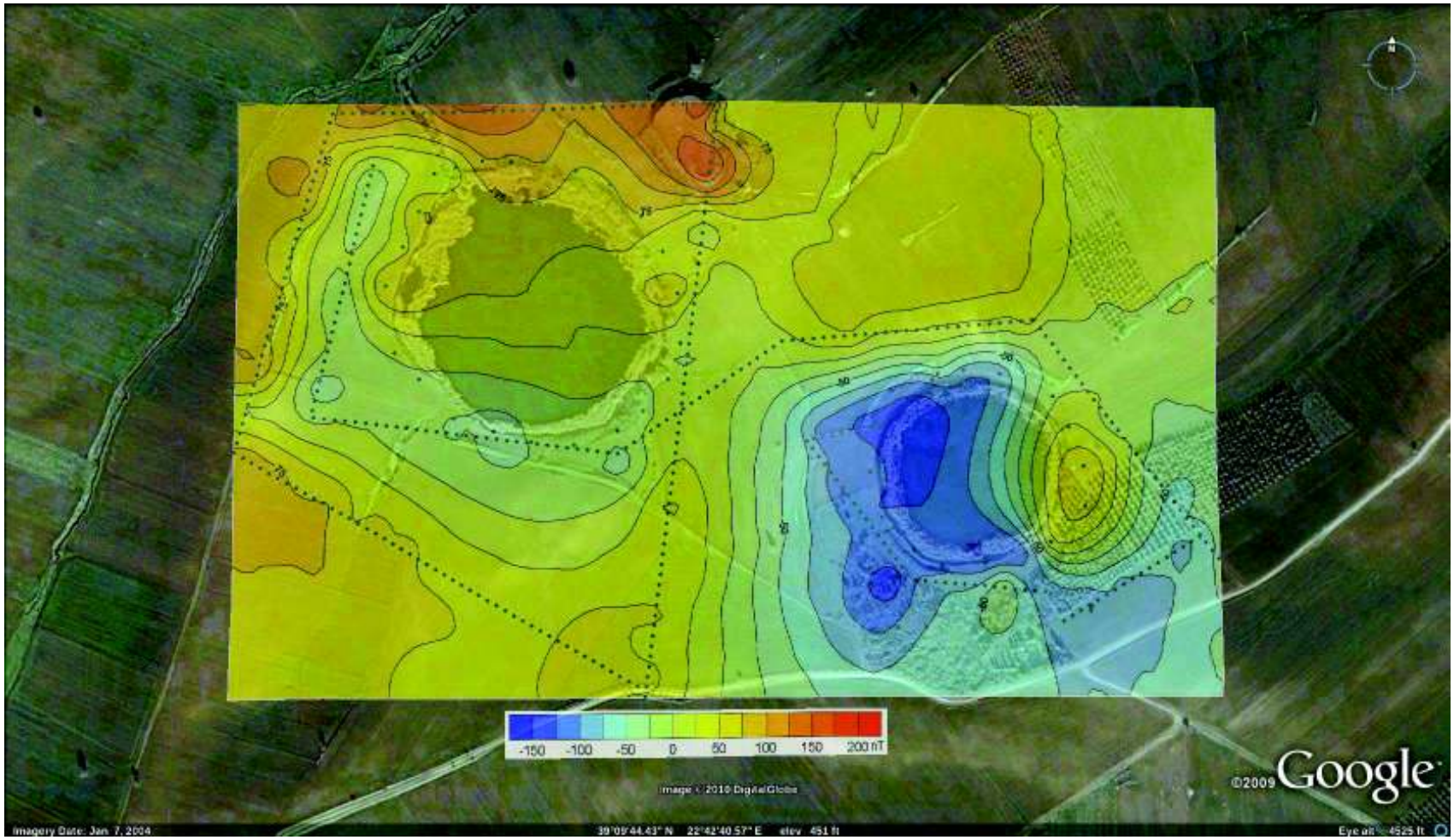

Figure 4.7. Total Field Magnetic Anomaly Map superimposed on the Google Image. Contour interval 25 nT. Stations are represented as dots.

References

Ernstson, K., Fiebag, J. 1992, The Azuara impact structure (Spain): new insights from geophysical and geological investigations, Geologische Rundschau, 81(2), 403-427.

Kord Ernstson (2010): Der Chiemgau-Impakt. Ein bayerisches Meteoritenkraterfeld (The Chiemgau Impact. A Bavarian Meteorite Crater Field - in German). 80 pages.

CHAPTER 5

DISCUSSION AND CONCLUSIONS

The working hypothesis of the origin of the Zerelia twin-lakes due to meteorite impact was based on the finding a considerable amount of angular to rounded clasts and polygenic breccias in the sandy-silty clay of their shores as well as in their suspicious halos during reconnaissance investigations. The lakes were regarded as dolines due to the occurrence of karst phenomena in the equivalent tectonic units in the surrounding Othris Mountains. Another hypothesis as volcanic maar-type diatremes has been suggested on the basis of the existence of small Cenozoic volcanic centers in the wider area (Marinou 1962), however without any evidence for ejected volcanic material.

Therefore, the major goal of the project was to find remnants of the meteorite, to investigate the underground structure of the lakes by geophysical methods in order to verify the hypothesis of their impact crater shapes and to find mineralogical evidence of high-temperature and high-pressures shock metamorphism.

The results of the mineralogical, petrographic and chemical studies and geophysical investigations will be discussed in this chapter, in order to clarify the origin of the lakes and to understand the condition of formation of the polygenic breccias and clast, which differ completely from all other rock formations of the underground.

The morphology and dimensions of the Zerelia lakes limit the physical conditions of a hypervelosity meteorite impact. According to the knowledge from all known and well established meteorite impact structures (compilation in Osinski et al., 2008; French, 1998 and in the “Earth Impact Database”), the dimensions of the meteorite, which might have split into two fragments, could have been about 10-30 m before reaching the surface.

5.1. METEORITE IMPACT CONDITIONS

Typical velocities for asteroids are 15–25 km/s when they enter the Earth atmosphere. Comets tend to have higher encounter velocities, e.g., as much as 60 km/s for Comet Halley. At such

speeds, these objects release all their energy when they strike the Earth. Because impact velocities are high, the kinetic energy of even small objects is also high. A stony meteorite only 6 m in diameter, colliding with the Earth at 20 km/s speed, forms a crater of approximate 120 m and releases an energy 8.3 x 10^{13} joules (J) equivalent to 20,000 tons of TNT or the effect of an „Hiroshima-type“ atomic bomb (compilation in French 1998). The impact of a projectile with a diameter of 23 m, forming a crater of 450 m, releases in seconds the energy of 1 Megaton TNT or 1 hydrogene bomb equivalent to 4.2 x 10^{15} J.

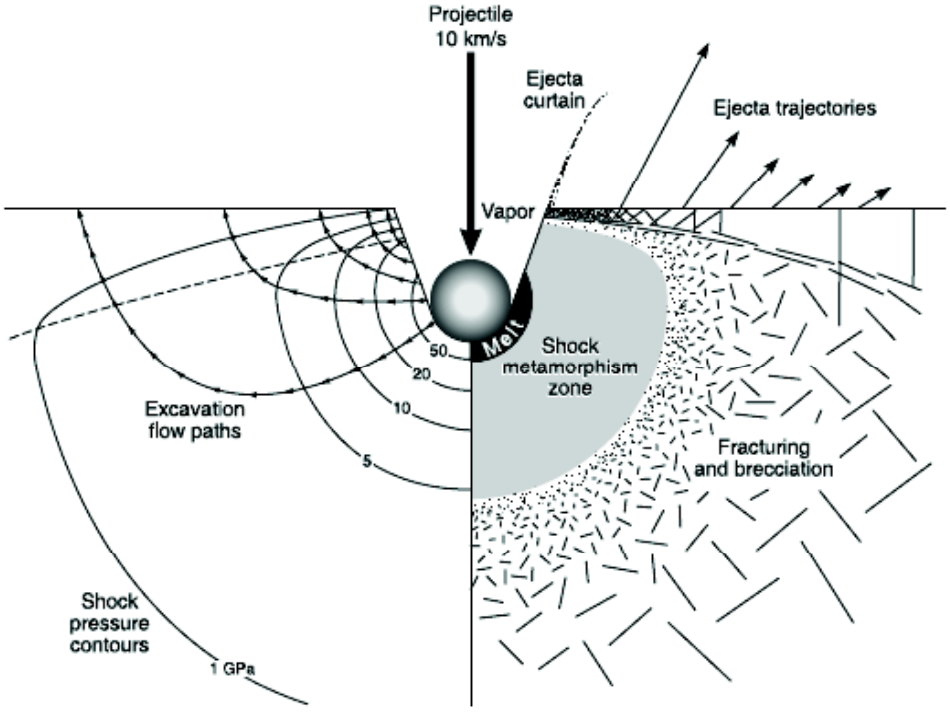

Figure 5.1 Contact/compression effects of a meteorite impact: initial shock-wave pressures and excavation flow lines around impact point (French 1998): max. shock pressure isobars in GPa, developed in the target around the impact point near the end of the contact/compression stage. The originally spherical projectile, after penetrating into the target, will be in most cases completely destroyed and converted to melt and vapor. Shock waves radiating from the projectile-target interface decline rapidly outward in peak pressure (isobars in GPa 1 to 50), creating concentric, approximately hemispherical zones of distinctive shock effects. From the original interface outward, these zones involve: (1) melting (>50 GPa) and formation of a large melt unit; (2) shock-deformation effects (5–50 GPa); (3) fracturing and brecciation (1–5 GPa). The subsequent excavation involves two processes: (1) upward ejection of large near-surface fragments and smaller ejecta; (2) subsurface flow of target material to form the transient crater with allochtonous debris fillings. (arrow paths crossing isobars at left side).

For the case of a hypothetical origin of the Zerelia twin-lakes due a meteorite impact, the above cited observations bracket the physical conditions of an impact. The general

contact/compression effects of a meteorite impact are shown in Fig. 5.1. For the rather small dimensions of the Zerelia lakes only low impact pressures of 1–5 GPa might be estimated based on the observed textural phenomena and the mineral composition of the carbonatitic breccias, which lead only to fracturing and brecciation.

5.2. PHASE RELATIONS OF $CACO_3$ AND IMPLICATION FOR IMPACT CONDITIONS

Osinski et al. (2008) reviewed experimental evidence and phase equilibria and synthesized these data sets with textural and mineralogical results of shock-metamorphed carbonates from the underground of several meteorite craters. Shock experiments on carbonates so far provide contrasting and ambiguous results.

Phase relations of $CaCO_3$ (Fig. 5.2) in the context of shock compression and decompression have been re-evaluated by Ivanov and Deutsch (2002). The main result of their work has been the extension of the liquid field of $CaCO_3$. This implies that the suspected result of hypervelocity impact with pressures > 1Gpa and temperatures between >1500 and 2000 K into carbonate sedimentary rocks is melting, with decomposition only occurring during post-shock cooling and decompression.

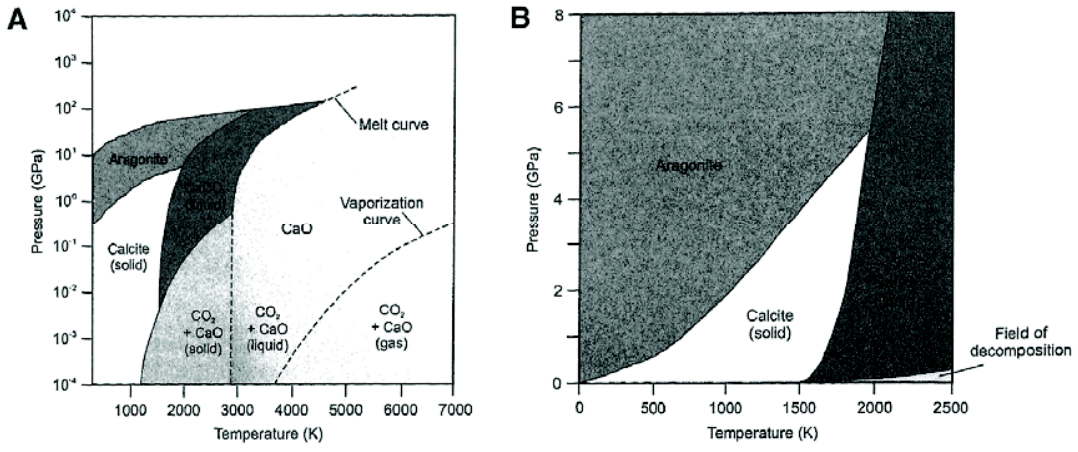

Figure 5.2 A: Phase diagram after Ivanov and Deutsch (2002) for $CaCO_3$ in log temperature/pressure plane. B: Expanded left middle part of $CaCO_3$ phase diagram shown in A. The diagram is plotted in linear coordinates to reveal the geometry of the phase boundaries.

Very high-post-shock temperatures close to the point of impact may result in vaporization of the carbonates (Tyburczy & Ahrens 1986), as it will be the same case for all rock types. The Phase relations of $CaCO_3$ that a limited decomposition from $CaCO_3$ melt may be possible following decompression. However, no evidence has been found in the Zerelia impact breccias.

Impact-generated melts occur in two main forms within impact craters: (1) as crystallized and/or glassy coherent impact melt sheets or layers within allochtonous crater fill-deposits (Fig. 5.4) and (2) as discrete glassy clasts within the crater fill-deposits and ejecta It has been found that the volume of impact melt in sedimentary and in mixed sedimentary-crystalline underground is about two orders of magnitude less than for pure crystalline targets in comparable sized meteorite craters (Kieffer & Simonds 1980). The reason for this phenomenon is that the enthalpies of H_2O-bearing and carbonate systems are such that a much smaller proportion of admixed sedimentary rocks than of anhydrous crystalline rock is required to quench the melt to subsolidus temperatures (Kieffer & Simonds 1980).

5.3. CONDITIONS OF SHOCK-METAMORPHISM

A compilation of the conditions of shock-metamorhism during impact of meteorites and the distinction from metamorphic processes in the Earth crust is given by French (1998) and shown in Fig. 5.3. It is important to note the temperatures of decomposition of zircon as well as melting of quartz to lechatallierite and sphene.

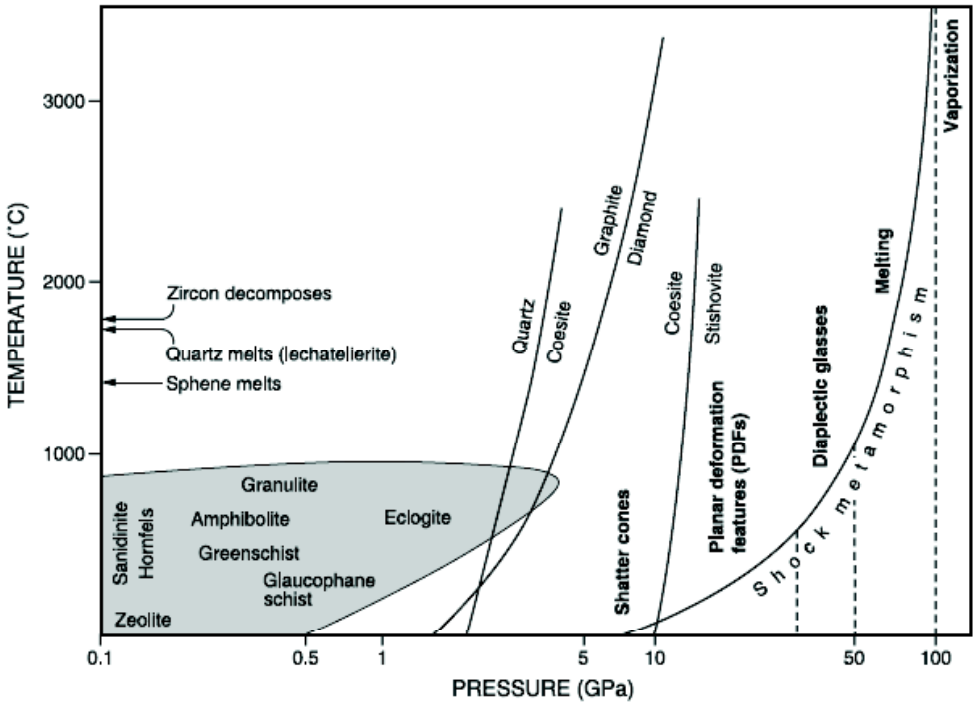

Figure 5.3. Conditions of shock-metamorphism. Pressure-temperature plot showing comparative conditions for shock-metamorphism and regional and contact metamorphism in the crust, The pressure X-axis in GPa is logarithmic. Shaded region at lower left (P < 5 GPa, T < 1000°C) encloses the metamorphic facies distribution. Shock-metamorphic conditions (at right) extend from ~7 to >100 GPa and are clearly distinct from metamorphic conditions in the crust. Approximate physical conditions for specific shock effects are indicated by vertical dashed lines, and the exponential curve ("Shock metamorphism") indicates the approximate postshock temperatures produced by specific shock pressures in granitic crystalline rocks. Relatively high shock pressures (>50 GPa) produce extreme temperatures, accompanied by unique mineral decomposition reactions (at left, near temperature axis). Stability curves for high-pressure minerals (coesite, diamond, stishovite) are shown for static equilibrium conditions.

5.4. HYPOTHETICAL SEQUENCE OF SHOCK-METAMORPHIC EFFECTS DURING THE ZERELIA METEORITE IMPACT

A hypothetical sequence of shock-metamorphic effects during the Zerelia meteorite impact is proposed on all the data obtained during the project. It should be noted, that up to now, no trace of the projectile (stone or iron meteorite) has been found.

5.4.1. Vaporization and partial melting of the underground Cretaceous sediments.

Carbonates with layers and lenses of silex (dense ultrafine quartz assemblages), conglomerates, shales and cherts (dense radiolarian cherts) were subjected to vaporization and partial melting during the impact and excavation, generating a huge blast in the order of seconds. Pressures may not have exceeded approximately 5 MPa, since neither diagnostic

PDFs (Planar Deformation Features) are presenrt in all quartz fragments nor high pressure polymorphs of quartz, such as coesite and stishovite as well as of zircon (reidite) or sphene have not yet been detected. High temperature polymorphs of quartz, tridymite and cristobalite may have been most probably transformed to normal low temperature α-quartz during hydrothermal alteration and deposition of the breccias and cooling.

The most convincing evidence for high temperature partial melting is the finding of irregular shaped decomposed „partial melted“ zircon and quartz, for which temperatures of >1400°–1800°C are required, which are not reached in metamorphic and magmatic processes within the Earth's crust and the uppermost mantle.

5.4.2. Transformation of $CaCO_3$ from vapor through liquid to solid state calcite

The „impact blast“ must have undergone, instantly and subsequent to the impact, transformations of heterogenous stages of lower pressures and temperatures. Experimental evidence and phase equilibria of $CaCO_3$ imply that carbonate sedimentary rocks can melt and and undergo vapor and liquid stages to quenched solid stage with decompositions of "mixed carbonate-silica melts" during post-shock cooling and decompression. This process is supported by the feathery to spinifex textures of the "sedimentary carbonatites", as well as documented by the heterogenous chemical compositions yielding abnormal high compounts of SiO_2 and Al_2O_3 of the cryptocrystalline, microcrystallin matrices and altered, devitrified glass fragments.

5.4.3. Hydrothermal phase subsequent to impact

Hydrothermal processes must have occurred subsequent to the impact within the crater fillings as well as in the ejecta during deposition. This is evident by the presence of different generations of calcite veins in the globules and clasts in the fallback breccias. The disseminated textures of the veins suggest a rather fast and local heterogenous hydrothermal process, since the bigger and entirely spinifex and spherulitic cemented carbonatitic breccias do not exhibit pervasive hydrothermal alteration, the latter being typical in many volcanic environments.

5.4.4. Emplacement and deposition of impact ejecta

Emplacement and deposition of impact ejecta must have followed the impact within seconds.

Thus, fracturing, brecciation, and excavation as well as subseqent cristallization of calcite to quenched spinifex and spherulitic assemblages are generated by a single instant event

compared to many other known geological processes, which can produce similar products mainly within multiple events, such as volcanic pyroclastic deposits or hydrothermal hydroclastic ejecta. Meteorite impact ejecta may differ in distribution and size around an impact structure (Fig. 5.4): mega to larger clasts, molten and quenched glassy fragments within the crater fillings and in the proximal walls, whereas smaller brecciated clasts, globular clasts and especially tectites are deposited in proximal environments.

A general model of a typical simple impact crater (Fig. 5.4) has been given by French (1998), which represents a compilation of numerous investigation during the past fifty years.

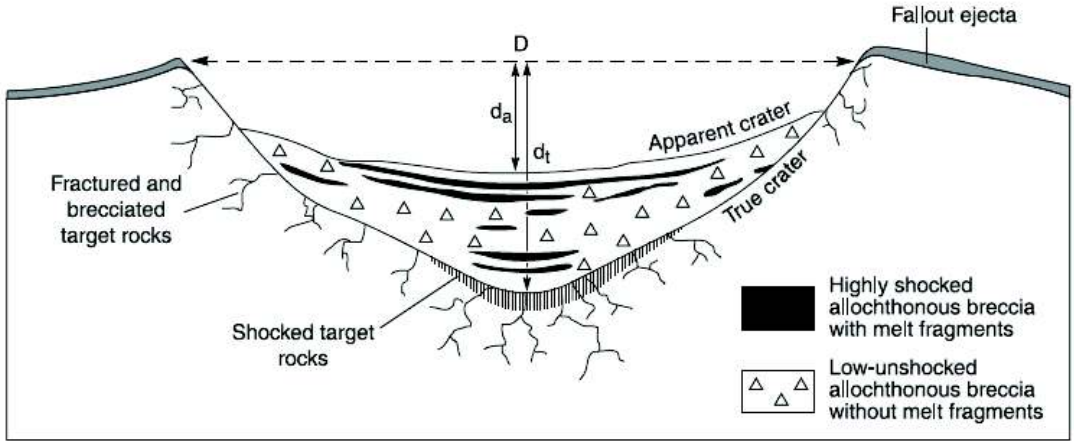

Figure 5.4. Typical impact structure showing the simple bowl shape and the locations of various types of impactites in and around the structure (compilation after French 1998). The basement rocks below the true crater floor are fractured and brecciated but generally show no distinctive shock effects, except in a small zone (fine vertical lines) in the center of the structure. The crater is filled, to approximately half its original height, with a variety of breccias and impact melts in form of lsmall lenses. A thin layer of ejected material (fallback breccias) overlies the uplifted crater rim (halo) and surrounds the crater. D = final crater diameter, which is in general 10–20% greater than the diameter of the original, premodification transient crater; dt = true depth of the final crater, which is approximately the depth of the original transient crater; da = apparent depth of the crater, or the depth from the final rim to the top of the crater-fill units.

5.5. CONCLUSIONS

Taking geological, mineralogical, petrographic, chemical and geophysical results of the investigation before and during the project into consideration, the most plausible answer for the origin of the Zerelia lakes is that of a meteorite impact origin.

Any other origin of the formation of the Zerelia lakes can be excluded: (1) an origin as dolines by karst formation. Circular lakes and steep holes of similar dimensions occur in many Greek areas within karst environments and limestone formations of different geological ages. Typical doline lakes are distributed in the area between Vonitsa and Lefkada. The walls of the lakes are steep and show no alteration and polygenic brecciation effects, the water-depth varies saisonally dramatically; (2) a hydrothermal, hydroclastic explosiv origin. Such craters are formed only in active volcanic fields with recent strong hydrothermal activity (e.g. Milos island). The whole Almiros plain and the entire neighbourhood of Zerelia lack of any sign of hydrothermal activity; (3) a Maar type, diatreme, volcanic explosion. Although also small volcanic tuff pipes occur in several volcanic field in intra-plate environments, even erupting carbonatitic magma from deep mantle depth, a comparison with the Zerelia lakes cannot be made. No other magmatic and volcanic material and relict mantle inclusions has been detected in the entire "backfall breccias". In addition the chaotic unconsolidated clastic sediments in the two outcrops in the wall of lake 2 did not show signs of sorting and stratification. Diatreme volcanic explosions occur always in multiple phases during hours and days, and therefore produce a certain layering within their surrounding tuff rings. Finally, the bulk chemical composition of the "Zerelia carbonatitic matrices" in the fallback breccia differs dramatically from the composition of magmatic carbonatitic globules from volcanic diatremes (e.g. from similar sized shape volcanic craters in the ultra-alkaline Province north of Rome).

Gravity profiles, modelling the extended areal of the western gravity anomaly (over the larger lake 2) show a small graben-type feature in a bowl form of a crater, extending at depths up to 200-250 m, as depicted by the density contrast tomography. Almost the same crater feature was also modelled for the eastern residual gravity anomaly over the eastern lake 1. The density contrast tomography indicates a crater extending at about a depth of 200-300 m. The form and shape of the above negative gravity anomalies are consistent with those in other areas of the world, where meteorite impacts occurred, as the Steinheim impact meteorite crater in southern Germany, and elsewhere.

The petrographic and chemical evidence of the consistent rock material as brecciated clasts and globules leads only to the interpretation as "impact fallback breccias and carbonatitic tectites" due to meteoritic impact, although up to now no meteorite fragments have been found. According to the size of the crater lakes and their close neighbourhood it can be

suspected that the projectile split into two fragments before reaching the surface. Their dimensions should have been between a few meters not exceeding 10 to 20 m. The temperature and pressure of their impact may have been sufficient to brecciate, partially vaporize and melt the limestones followed by quenching during cooling and decompression to form the carbonatitic clasts.

REFERENCES

Alvarez, L. W., Alvarez W., Asaro, F., & Michel, H. V. (1980): Extraterrestrial cause for the Cretaceous-Tertiary extinction. Science, 208, 1095–1108.

Alvarez, W. (1997): T. Rex and the Crater of Doom. Princeton Univ., Princeton. 185 pp.

Alvarez, W., Claeys, P. & Kieffer, S. W. (1995): Emplacement of Cretaceous-Tertiary boundary shocked quartz from Chicxulub crater. Science, 269, 930–935.

Brooker, R.A. (1998): The effect of CO_2 saturation on immiscibility between silicate and carbonate liquids: An experimental study. Journal of Petrology, Vol. 391905-1915.

Dietrich, V.J. & Gartzos, E. (2009): Twin meteorite impact craters in Thessaly (Central Greece) of Holocene age. Proceedings of the 7th Swiss Geoscience Metting, Neuchâtel, November 2009.

Duller, G.A.T. (2004): Luminescence dating of Quaternary sediments: recent advances. *Journal* of Quaternary science, 19, 183-192.

Earth Impact Database (last update December 12, 2010): Planetary and Space Science Centre, University of Brunswick, Canada.
http://www.passc.net/EarthImpactDatabase/index.html

French B. M. (1998) Traces of Catastrophe: A Handbook of Shock-Metamorphic Effects in Terrestrial Meteorite Impact Structures. LPI Contribution No. 954, Lunar and Planetary Institute, Houston. 120 pp.

French, B. M. & Koeberl, C. (2010): The convincing identification of terrestrial meteorite impact structures: What works, what doesn't, and why. Earth-Science Reviews 98 (2010) 123–170.

Graup, G. (1999): Carbonate-silicate liquid immiscibility upon impact melting: Ries Crater Germany. Meteoritics & Planetary Science, 34, 425-438.

Grieve, R.F.A., Langenhorst, F. & Stöffler, D. (1996): Shock metamorphism of quartz in nature and experiment, II: Significance in Geoscience. Meteoritics & Planetary Science 31, 6-35.

Hartung, M. (2006): More Evidence Chicxulub Was Too Early.

http://gsa.confex.com/gsa/06boa/finalprogram/abstract_101180.htm

Ivanov, B.A. & Deutsch, A. (2002): The phase diagram of $CaCO_3$ in relation to shock compression and decompression. Physics of the Earth and Planetary Interiors. Vol. 129, 131-143.

Jones, A.P., Langenhorst, Claeys, P. & Heuschkel, S. (2000): Impact melting of carbonates from Chicxulub Crater. In: Gilmour, L. & Koeberl., eds., Impacts and the Early Earth: Lecture Notes in Earth Sciences, 91. Springer Verlag, 343-361.

Keller, M. (2010): Die Sedimente der Zwillings-Impaktkraterseen in Thessalien, Griechenland. Semesterarbeit FS 2010, Dept. Environmental Sciences, ETH Zurich, Switzerland, 53p. (in German).

Kieffer S. W. & Simonds C. H. (1980) The role of volatiles and lithology in the impact cratering process. Rev. Geophys. Space Phys., 18, 143–181.

Koeberl C. & Anderson R. R., eds. (1996a) The Manson Impact Structure, Iowa: Anatomy of an Impact Crater. Geol. Soc. Amer. Spec. Paper 302. 468 pp.

Koerberl, C. & Henkel, H. (editors) (2005): Impact Tectonics. Springer Berlin Heidelberg New York, 552p., ISBN 3-540-24181-7.

Langenhorst, F. (2002): Shock metamorphism of some minerals: Basic introduction and microstructural obeservations. Bulletin of the Czech Geological Survey, Vol. 77, No. 4, 265-282.

Langenhorst, F., Deutsch, A., Ivanov, B.A. & Hornemann, U. (2000): On the shock behavior of $CaCO_3$: Dynamic loading and fast unloading experiments – modeling – mineralogical observations: Lunar and Planetary Science Conference, 31st, abstracts1851.

Marinos, G., Anastopoulos, J., Maratos, G., Melidonis, N. & Andronopoulos, B. (1962): Geological Map of Greece 1 : 50 000, Sheet Almyros. Institute for Geology and Subsurface Research, Athen.

Marinos, G., Anastopoulos, J., Maratos, G., Melidonis, N. & Andronopoulos, B. (1957): Geological maps of Greece, 1 : 50 000, sheet Anavra, Institute for Geology and Subsurface Research, Athen.

Marinou, G. (1962): Sur deux volcans embryonnaires du type mare, prés d'Almyros-Thessalie. Bulletin Geological Society of Greece, 5, 1, 108-114.

Osinski, G.R. (2005): Hydrothermal activity associated with the Ries impact event, Germany. Geofluids, Vol. 5, 202-220.

Osinski, G.R., Spray, J.G. & Grieve (2008): Impact melting in sedimentary target rocks: An assessment. In: Evans, K.R., Horton, J.W. Jr., King, D.T. Jr. & Morrow, J.R. eds., The Sedimentary Record of Meteorite Impacts. Geological Society of America Special Paper, 437, 1-8.

Osinski, G.R., Spray, J.G. & Lee, P. (2005): Impactites of the Haughton impact structure, Devon Island, Canadian High Arctic. c 1789-1812. Meteoritics & Planetary Science 40, Nr. 12, 1789-1812.

Pinto, J.A. & Warme,, J.E. (2008): Alamo Event, Nevada: Crater stratigraphy and impact breccia Realms. The Geological Society of America, Special Paper 437, 99-137.

Reinders, H.R. , Floras, S., Sgouvas, I. & co-workers (2004): Prehistoric Sites at the Almiros and Sourpi Plains (Thessaly, Greece). Royal Van Gorcum & Comp., B.O.Box 43, 9400 AAAssen, The Netherlands. ISBN 90 232 40 26X.

Shoemaker, E. M. & Chao, E. C. T. (1961): New evidence for the impact origin of the Ries Basin, Bavaria, Germany. Journal. Geophys. Res., 66, 3371–3378.

Stähle, V., Altherr, R., Koch, M. & Nasdala, L. (2008): Shock-induced growth and metastability of stishovite and coesite in lithic clasts from suevite of the Ries impact crater (Germany). Contr. Mineral. Petrol., 155, 457-472.

Stoppa, F. & Lupini, L. (1993): Mineralogy and petrology of the Polino Monticellite Calciocarbonatite (Central Italy). Mineralogy and petrology, 49, 213-231.

Taylor, G.J. (2009): Time to Solidify an Ocean of Magma. Planetary Science Research Discoveries (PSRD), March 25, 2009. http//www.psrd.hawaii.edu.Mar09/magmaOceanSolidification.html

Trepmann, C.A. (2008): Shock effects in quartz: Compression versus shear deformation – An example from the Rochechouart impact structure, France. Earth and Planetary Science Letters, 267, 322-332.

Tyburczy, J.A. & Ahrens, (1986): Dynamic compression and volatile release of carbonates. Journal of Geophysical Research, Vol. 91, 4730-4744.

von Engelhardt, W. & Stöffler, D. (1965): Spaltflächen im Quarz als Anzeichen für Einschläge grosser Meteoriten. Naturwissenschaften, 17, 489–490.

von Engelhardt, W. & Stöffler, D. (1968): Stages of shock metamorphism in crystalline rocks of the Ries Basin, Germany.In Shock Metamorphism of Natural Materials (B. M. Frenchand N. M. Short, eds.), 159–168. Mono Book Corp., Baltimore.